

NAG 1-1084  
IN-76-CR  
171778

**The Charles E. Via, Jr.  
Department of Civil Engineering** p.133

802224

**HYDROSYSTEMS  
ENGINEERING**

A Spectral Method Determination of the First  
Critical Rayleigh Number for a Low-Prandtl  
Number Crystal Melt in a Cylindrical Container

by

C.M. Dietz, Jr. and P. Diplas

July 1993

Sponsored by

National Aeronautics and Space Administration,  
Langley Research Center  
Center for Innovative Technology of Virginia

(NASA-CR-193238) A SPECTRAL METHOD  
DETERMINATION OF THE FIRST CRITICAL  
RAYLEIGH NUMBER FOR A LOW-PRANDTL  
NUMBER CRYSTAL MELT IN A  
CYLINDRICAL CONTAINER (Virginia  
Polytechnic Inst. and State Univ.)  
133 p

N93-29214

Unclass

G3/76 0171778

Blacksburg, VA 24061

Virginia



Tech

VIRGINIA POLYTECHNIC INSTITUTE  
AND STATE UNIVERSITY

A Spectral Method Determination of the First Critical Rayleigh  
Number for a Low-Prandtl Number Crystal Melt in a Cylindrical  
Container

by

C.M. Dietz, Jr. and P. Diplas

Sponsored by

National Aeronautics and Space Administration,  
Langley Research Center  
Center for Innovative Technology of Virginia

July 1993

HYDROSYSTEMS ENGINEERING

The Charles E. Via, Jr.  
Department of Civil Engineering  
Virginia Polytechnic Institute and State University  
Blacksburg, VA 24061

## ACKNOWLEDGEMENTS

Support for the present study was provided by the National Aeronautics and Space Administration (NASA) research grant NAG-1-1084, Langley Research Center, and the Center for Innovative Technology of Virginia research grant SPA-91-001. The title of this project was "Chaos and Crystal Growth: An Exploratory Study" and it was awarded to Dr. P. Diplas. The authors wish to express their appreciation to Dr. Archibald Fripp who arranged for a visit of the microgravity facilities at the Langley Research Center. He also provided a lot of technical information during the course of this study and reviewed an early draft of this paper.

## EXECUTIVE SUMMARY

The onset of laminar axisymmetric Rayleigh-Benard convection is investigated for a low-Prandtl number liquid metal in a cylindrical container. All surfaces are considered to be solid and no-slip. Two separate cases are examined for the thermal boundary conditions at the side wall, one with conducting and the other with insulated surface.

The governing Boussinesq system is first perturbed and then simplified by introducing a Stokes stream function. Subsequently, a Chebyshev Galerkin spectral model is employed to reduce the simplified system to a system of first-order nonlinear ordinary differential equations. A local stability analysis determines the two values of the first critical Rayleigh number,  $Ra_{c1}$ , for the insulated and conducting side walls.

As expected, the conducting  $Ra_{c1}$  value of 2882.5 obtained from the present approach exceeded the corresponding insulated  $Ra_{c1}$  value of 2331.6. For the insulated case, an earlier study using a different numerical approach suggests that  $Ra_{c1} = 2261.9$ , while an experimental study measured  $Ra_{c1} = 2700$ .

## **Table of Contents**

<b>Executive Summary.....</b>	<b>ii</b>
<b>Acknowledgments.....</b>	<b>iii</b>
<b>Table of Contents.....</b>	<b>iv</b>
<b>List of Figures.....</b>	<b>vi</b>
<b>List of Symbols.....</b>	<b>ix</b>

### **Chapter 1:**

<b>Introduction.....</b>	<b>1</b>
1.1 The Growth of Crystals from the Melt.....	3
1.2 The Vertical Bridgman Technique.....	6
1.3 The Solution Approach.....	8

### **Chapter 2:**

<b>Literature Review.....</b>	<b>15</b>
-------------------------------	-----------

### **Chapter 3:**

<b>Rayleigh-Bénard Convection.....</b>	<b>24</b>
3.1 The Physics of Rayleigh-Bénard Convection.....	24
3.2 The Boussinesq System.....	27

### **Chapter 4:**

<b>The Chebyshev-Galerkin Spectral Method.....</b>	<b>39</b>
4.1 Perturbation of the Boussinesq System.....	41

4.2 Simplification of the Perturbed Boussinesq System.....	43
4.3 Chebyshev Series Representation of Dependent Variables.....	47
4.4 Chebyshev-Galerkin Spectral Method.....	59
 <b>Chapter 5:</b>	
Local Stability Analysis.....	81
5.1 Local Bifurcation Theory.....	82
5.2 Stationary Solutions.....	84
5.3 The Linear Approximation.....	89
 <b>Chapter 6:</b>	
Discussion of Results.....	105
 <b>Chapter 7:</b>	
Conclusion.....	108
 References.....	 111
 <b>Appendix A:</b>	
Local Stability Analysis, Insulated Side Wall.....	115

## List of Figures

Figure 1: Conductive (Diffusion-controlled) and convective (Completely-mixed) concentration profiles for a two-component melt (Knuteson, 1989).....	10
Figure 2: Flow regime transitions as a function of Prandtl number (Krishnamurti, 1973).....	11
Figure 3: Vertical Bridgman apparatus (Knuteson, 1989)....	12
Figure 4: Sample placement of thermocouples on ampoule in the Bridgman furnace (Knuteson, 1989).....	13
Figure 5: Temperature vs. time graph for periodic flow field in a crystal melt. The TC-# indicates the particular thermocouple (Knuteson, 1989).....	14
Figure 6: Rayleigh-Bénard convection in a fluid column. $T_2 > T_1$ .....	36
Figure 7: Parallel laminar convection rolls in a closed rectangular box with slip side walls. The convective redistribution of heat is evident from the temperature gradients in the fluid layer (from Shirer, 1987).....	37
Figure 8: Axisymmetric convection roll in cylinder of aspect ratio one (from Müller et al., 1984).....	38
Figure 9: Toroidal shape of axisymmetric convection cell..	68
Figure 10: Laminar axisymmetric flow field, $\gamma=1$ , for water (Pr=6.7) ( Müller et al., 1984).....	69

Figure 11: r-variation of $v_z$ .....	70
Figure 12: r-variation of $v_r$ .....	71
Figure 13: z-variation of $v_r$ .....	72
Figure 14: z-variation of $v_z$ .....	73
Figure 15: Axisymmetric flow field for $\psi(r,z)$ in half-section of cylinder with $\gamma=1$ . Flow rotates counterclockwise, falling at the center.....	74
Figure 16: r-variation of conducting $T^1(r,z,t)$ expression.....	75
Figure 17: z-variation of conducting $T^1(r,z,t)$ expression.....	76
Figure 18: r-variation of insulated $T^1(r,z,t)$ expression.....	77
Figure 19: z-variation of insulated $T^1(r,z,t)$ expression.....	78
Figure 20: r-variations of insulated, conducting $T^1(r,z,t)$ expressions.....	79
Figure 21: z-variation of $T^2(r,z,t)$ expression.....	80
Figure 22: Bifurcation diagram for $\psi_{54}(t)$ , conducting side wall.....	99
Figure 23: Bifurcation diagram for $T_{34}(t)$ , conducting side wall.....	100
Figure 24: Bifurcation diagram for $T_{03}(t)$ , conducting side wall.....	101
Figure 25: Bifurcation diagram for $\psi_{54}(t)$ , insulated side wall.....	102
Figure 26: Bifurcation diagram for $T_{54}(t)$ , insulated side wall.....	103

Figure 27: Bifurcation diagram for $T_{03}(t)$ , insulated side wall.....	104
Figure 28: Graph from Müller et al. (1984) showing the flow regimes and transitions for liquid gallium.....	107

### List of Symbols

$a$ ,	coefficient of $v_z(r)$ polynomial expression
$a_i$ ,	Chebyshev series coefficient
$a_k$ ,	temporal component of separation of variables expression
$b$ ,	coefficient of $v_z(r)$ polynomial expression
$b_i, b_j$	Chebyshev series coefficients
$C$ ,	constant
$C_1, C_2$ ,	constants
$C_v$ ,	heat capacity at constant volume, per unit mass
$\mathbb{C}$ ,	complex number set
$c$ ,	coefficient of $v_z(r)$ polynomial expression
$c_1, c_2$	constants
$c_k$ ,	Chebyshev series coefficient
$d$ ,	coefficient of $v_z(r)$ polynomial expression
$d_1$ ,	Chebyshev series coefficient
$e$ ,	coefficient of $v_z(r)$ polynomial expression
$\hat{e}_z$ ,	unit vector in the $z$ -direction
$\hat{e}_\theta$ ,	unit vector in the $\theta$ -direction
$f_1, f_2$	mathematical expressions
$g$ ,	acceleration of gravity = $(g_r, g_\theta, g_z)$
$h$ ,	height of the cylinder
$J$ ,	Jacobian
$K$ ,	Kelvin

$L$ , length of the container  
 $M$ , representation of time-independent terms of Boussinesq system  
 $N$ , number of terms in the finite series approximation of the Boussinesq system  
 $n$ , dimension of real number space; degree of Chebyshev function  $T_n(x)$   
 $p$ , pressure  
 $p_2$ , pressure at the bottom boundary  
 $Pr$ , Prandtl number =  $\nu/\kappa$   
 $q$ , energy flux relative to mass average velocity  
 $R$ , radius of cylinder  
 $\mathbb{R}$ , real number set  
 $r$ , radial coordinate  
 $Ra$ , Rayleigh number =  $\frac{g\alpha\Delta Th^3}{\nu\kappa}$   
 $Ra_{c1}$ , first critical Rayleigh number  
 $T$ , temperature  
 $T^1$ , first term in the Chebyshev series expansion  
 $T^2$ , second term in the Chebyshev series expansion  
 $T_1$ , temperature at the top boundary  
 $T_2$ , temperature at the bottom boundary  
 $T_{ij}$ , temporal term in the Chebyshev expansion. The subscripts  $i$  and  $j$  indicate the highest degree of the

Chebyshev series expansion for the  $r$  and  $z$  distributions, respectively

$\Delta T,$	temperature gradient = $T_2 - T_1$
$T_n,$	Chebyshev function of degree $n$
$t,$	time
TC,	thermocouple
$u,$	Boussinesq solution vector
$u_k,$	spatial component of separation of variables expression
$v,$	velocity vector = $(v_r, v_\theta, v_z)$
$x$	x-coordinate
$x,$	solution vector
$\bar{x},$	stationary solution vector
$z,$	vertical coordinate

#### Greek Symbols

$\alpha,$	volumetric thermal expansion coefficient
$\gamma,$	aspect ratio = $h/R$
$\delta_{kl}$	Kronecker delta
$\theta,$	angular coordinate
$\kappa,$	thermal diffusivity
$\lambda$	eigenvalue
$\mu,$	dynamic viscosity
$\nu,$	kinematic viscosity

$\rho$ , fluid density  
 $\rho_0$ , reference fluid density  
 $\tau$ , viscous stress tensor  
 $\tau_{ij}$ , viscous stress tensor component  
 $\phi$ , test function  
 $\psi$ , Stokes stream function

#### Superscripts

$I$  insulated side wall case  
 $N$  number of terms in Chebyshev series decomposition  
 $P$ , convective perturbation  
 $S$ , stationary convective solution  
 $*$ , nondimensional variable in the unperturbed Boussinesq system  
 $^{*}$ , nondimensional conductive perturbation  
 $^{\wedge}$ , coefficient of exponential convective perturbation

#### Subscripts

$0$ , conductive basic state  
 $^{\wedge}_V$ , at constant volume

#### Special Symbols

$( : )$ , scalar product of tensors

## CHAPTER 1. INTRODUCTION

The homogeneity of semiconductor crystals is a primary concern of the electronics industry. The refinement of techniques for controlling the composition of semiconductor crystals during growth has been an integral part of recent advances in electronic microcircuitry. The difficulties and compromises inherent in growing homogeneous crystals have given impetus to both theoretical and experimental efforts to gain a better understanding of crystal growth phenomena. Recent theoretical work in the fields of nonlinear dynamics and stability theory has been promising in determining the onset of flow patterns in the liquid that affect the homogeneity of the resulting crystal. The computational difficulties of modeling a fluid on the route to turbulence remain formidable, however.

Convection is the governing phenomenon in a number of crystal growth methods (e.g., Ostrach, 1983). It is present in a wide variety of natural and industrial processes, among them some of interest to civil engineers. Thermal instabilities in the atmosphere (e.g., Lorenz, 1963) and in the borders of lakes (e.g., Horsch, 1988) are the product of convective forces. Secondary currents in stream meanders have

some similarities to the convection rolls present in the laminar regime of buoyancy-driven convection, the difference being one of exchange of momentum rather than heat. The study of convection in the more controlled conditions of crystal growth allows a better understanding of its effects in these other more complicated phenomena.

A single semiconductor crystal can be formed from a liquid alloy, or melt, in the presence of a vertical differential temperature gradient. Although the most common configuration has a higher temperature at the top of the melt than at the bottom, the most interesting fluid phenomena are found in the "hot-on-bottom" configuration (e.g., Ostrach, 1983). The "hot-on-bottom" configuration is the case considered in the present study.

The transfer of heat in the melt is controlled by conduction or by some form of convection, depending upon the strength of the temperature gradient. The physical properties of the crystal depend upon the type of heat transfer and the flow field in the melt during growth (Kim et al., 1972). The effect of convection on the crystal composition depends upon the degree of mixing in the melt (e.g., Müller et al., 1984). It is therefore possible to obtain some measure of control of the composition of the crystal by varying the flow pattern in the melt. Determining the particular flow regime in the melt at any time is a matter of determining the temperature

gradient at the onset of each of the different convective flow regimes.

Single semiconductor crystals formed from alloys containing metals are a class of crystals with important industrial applications. Crystals such as lead-tin-telluride (LTT) have light-sensitive properties that have made possible the development of night-vision devices (Parker and Johnson, 1981). These crystals have unique problems associated with their growth. Because a melt containing a metal may be highly sensitive to changes in the temperature gradient (Krishnamurti, 1973), control of the growth of the crystal can be problematic. In an effort to delineate the different flow regimes in such a melt, it is the purpose of the present study to determine the onset of the transition between the conductive and laminar convective regimes.

### **1.1 The Growth of Crystals from the Melt**

There are a number of forces involved in the growth of a crystal. In a multi-component melt, convection may be induced by instabilities that are solutal as well as thermal (Crouch et al., 1985). In the absence of surface tension effects and

any horizontal temperature gradients, the flow in the melt is strictly some form of Rayleigh-Bénard (buoyancy-driven) convection (e.g., Charlson and Sani, 1970).

Creating a multi-component crystal that is homogeneous can be an elusive undertaking. Although it is possible to grow a crystal in either a conductive or a convective flow regime, each heat transfer mechanism induces certain phenomena that create difficulties in controlling homogeneity. Under purely conductive heat transfer conditions, a multi-component crystal with a nearly constant concentration profile (Fig. 1) can be produced. The homogeneity of this crystal results in uniform electrical properties. However, large axial temperature gradients are necessary to avoid constitutional supercooling and dendritic growth at the crystal-melt interface (Tiller et al., 1953 and Mullins and Sekarka, 1964). Sufficiently large axial temperature differences induce large radial temperature differences that are inherently destabilizing and initiate convection (e.g., Tritton, 1988). Convection that is unsteady produces a varying concentration profile in a multi-component melt (Fig. 1). The more vigorous the convective mixing, the greater the occurrence of backmelting at the melt-crystal interface and the possibility of the formation of striations of differing compositions (e.g., Kim et al., 1972). Determination of the axial temperature gradients at which the flow regime transitions

occur is therefore essential for balancing the deleterious effects of these two heat transfer mechanisms.

In the present study the melt consists of the single component tin. In a single-component melt only thermal instabilities are significant, allowing this type of instability to be examined without the interference of most of these other complex phenomena.

The specific response of the liquid melt to the forcing temperature gradient depends upon three parameters: (1) the strength and orientation of the temperature gradient, measured by the nondimensional Rayleigh number,  $Ra$ , (2) the relative rates of molecular diffusion of heat versus momentum by the fluid, measured by the Prandtl number of the fluid,  $Pr$ , and (3) the relative dimensions or aspect ratio  $\gamma$  of the fluid container as well as its shape (e.g., Higgins, 1987). For a given fluid and container geometry, as the Rayleigh number is gradually increased, the melt passes from the conductive heat transfer state through a sequence of convective flow regimes: laminar, periodic, quasiperiodic, and turbulent (Krishnamurti, 1973). The Rayleigh numbers at which these transitions or Rayleigh instabilities occur are called critical Rayleigh numbers.

The liquid metals used to grow semiconductor crystals are characterized by low Prandtl numbers, typically less than 0.5 (e.g., Knuteson, 1989). Flow regime transitions for these

low-Prandtl number fluids occur over a narrower range of Rayleigh numbers compared to fluids of higher Prandtl number (Krishnamurti, 1973) (Fig. 2). In the present study, a tin melt of Prandtl number 0.01 is heated from below in a closed cylindrical container with height equal to its radius. The first critical Rayleigh number marking the onset of the transition from conduction to the laminar convection regime for this set-up is determined. Although this critical Rayleigh number is independent of the Prandtl number and consequently of the fluid (e.g., Krishnamurti, 1973), the techniques used in this study illustrate the basic method in the determination of the entire series of critical Rayleigh number values for a buoyancy-driven flow.

### **1.2 The Vertical Bridgman Technique**

A common method for growing single crystals is the vertical Bridgman technique (e.g., Carlson et al., 1984). In the "top-down" vertical Bridgman configuration, a cylindrical ampoule of the liquid metal is moved upward through a linear vertical temperature gradient that is hotter on the bottom (Fig. 3). The sides surrounding the ampoule are insulated, and the top and bottom surfaces of the ampoule are conducting. The crystal grows from the top of the ampoule down. The shape

of the crystal-melt interface is curved, with the fastest growth generally occurring at the sides. The Bridgman apparatus effectively makes the melt a closed system, so that there are no free surfaces and no destabilizing surface tension gradients.

The enclosed nature of the Bridgman furnace setup (Fig. 3) as well as the opacity of liquid metals do not permit the usual flow visualization techniques in the experimental apparatus. Instead, other techniques have been developed to assist in the determination of the temperature and velocity patterns for a liquid metal during a crystal growth experiment. For example, thermocouples arranged systematically about the cylindrical ampoule (Fig. 4) allow a temperature time series to be recorded (Fig. 5). Deviations from the stationary conductive linear temperature gradient permit the large-scale temperature variations to be detected. Because of the correlation between the temperature and velocity fields, especially in the vertical direction, an approximation to the large-scale flow field can be determined experimentally. This approximation is useful because it is precise enough to indicate the type of convective flow regime present. The Rayleigh instabilities may be found at the temperature gradients where there is a distinct and stable qualitative change in the temperature and flow fields.

### 1.3 The Solution Approach

In the present study, the onset of laminar axisymmetric convective flow of liquid tin in a cylindrical container whose radius is equal to its height is investigated. The crystal-melt interface is assumed to be planar. The height of the melt column is considered to be constant for the time scale of the study. The flow is considered to be axisymmetric, producing a rotational flow field in the shape of a torus. Because of the rigid surfaces of the container, the velocity is required to satisfy the no-slip condition--attain a zero value--at the solid boundary. For the thermal boundary conditions, the top and bottom are conducting faces. The side wall is insulated in the vertical Bridgman technique, but both insulated and conducting cases are considered in the present study as a check upon the validity of the model. Because of the loss of heat through a conducting side wall, the temperature gradient and critical Rayleigh number necessary to initiate convection should be higher than for the insulated case.

In the present study, a Chebyshev-Galerkin spectral method is used to transform the governing nonlinear system of partial differential equations into a low-order nonlinear system of ordinary differential equations. A local stability analysis of this system is used to determine the first

critical Rayleigh number.

In the present work, the problem is viewed first from a physical perspective. In Chapter 3, the notion of physical stability in Rayleigh-Bénard convection is explored, and the assumptions of the governing Boussinesq system are investigated. In Chapter 4, the Boussinesq system is perturbed and simplified. The dependent variables are represented by finite Chebyshev series, and a Galerkin spectral method is used to transform the Boussinesq system into an approximate system of first-order ordinary differential equations.

In Chapter 5, the two types of instabilities of a mathematical system are examined. The nonlinear system is perturbed, linearized, and put into variational form. The conditions under which linear analysis of a nonlinear system is valid is presented. Such a linear analysis based upon the eigenvalues determines the critical Rayleigh number at the transition from conduction to laminar convective flow. Both insulated and conducting side walls are considered.

The results are compared to a numerical study by Charlson and Sani (1970), who found the first critical Rayleigh number for the onset of laminar convection for both thermal boundary conditions for a range of aspect ratios. The results are also compared to the experimental results of Müller et al. (1984) for liquid gallium.

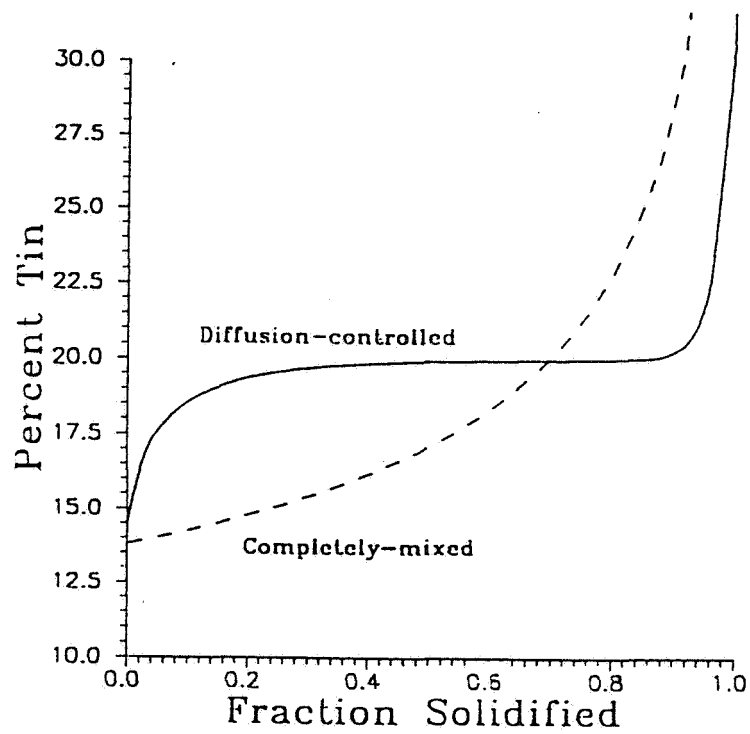


**Figure 1.** Conductive (Diffusion-controlled) and convective (Completely-mixed) concentration profiles for a two-component melt (Knuteson, 1989).

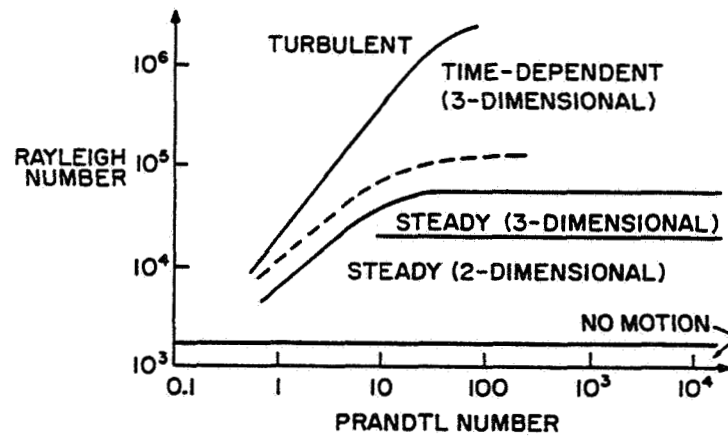


**Figure 2.** Flow regime transitions as a function of Prandtl number (Krishnamurti, 1973).

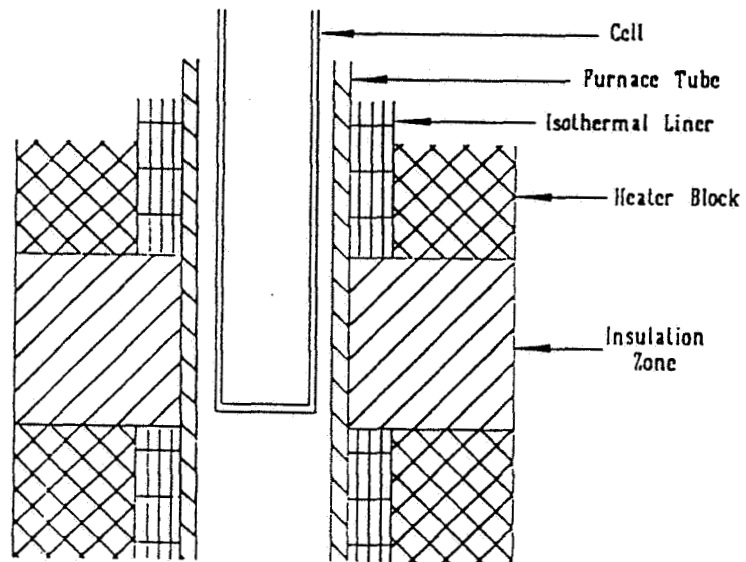


**Figure 3.** Vertical Bridgman apparatus (Knuteson, 1989).

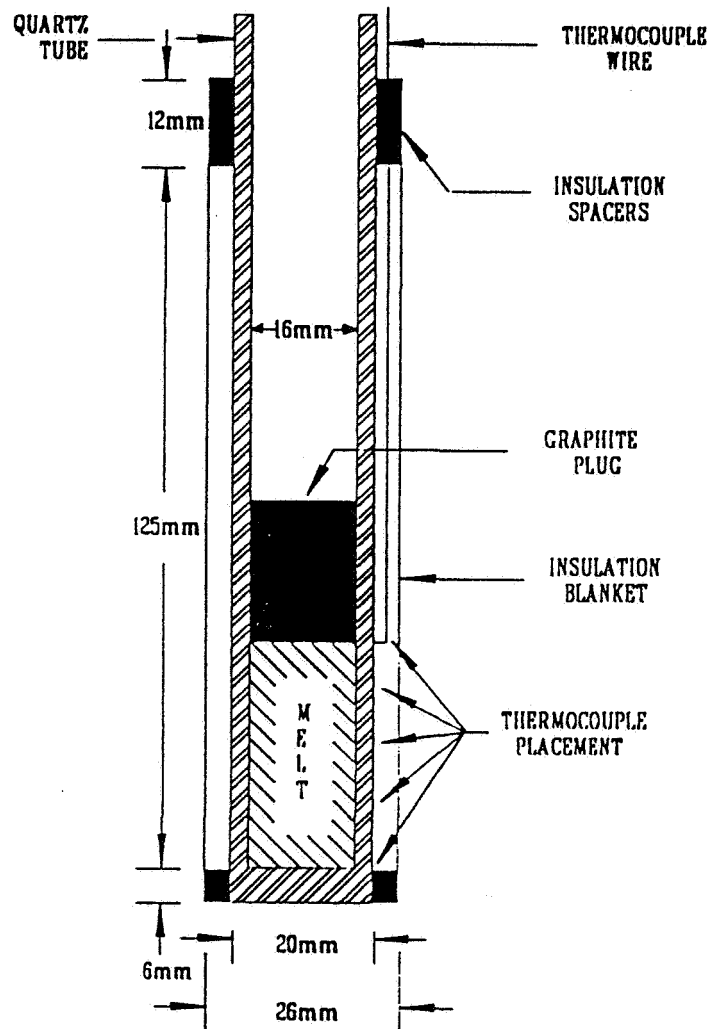


**Figure 4.** Sample placement of thermocouples on ampoule in the Bridgman furnace (Knuteson, 1989).

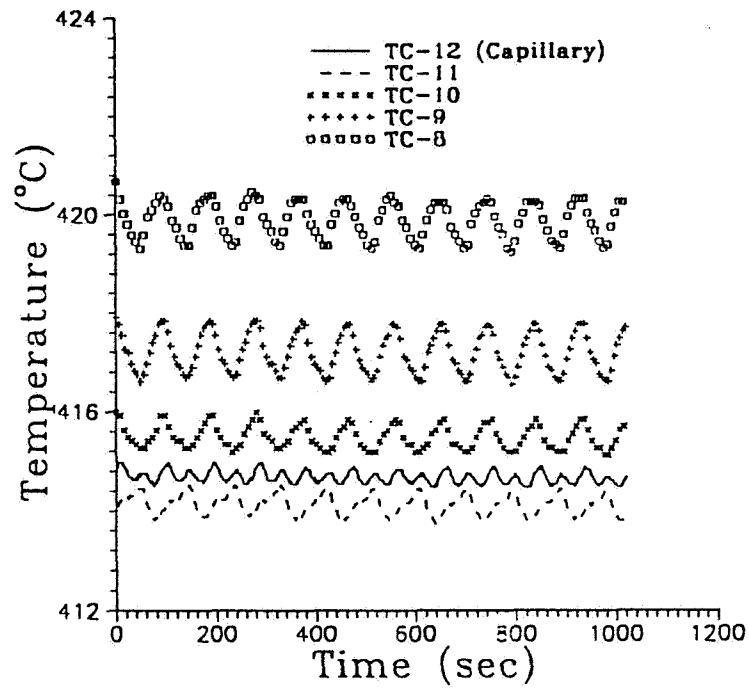


**Figure 5.** Temperature vs. time graph for periodic flow field in a crystal melt. The TC-# indicates the particular thermocouple (Knuteson, 1989).

## CHAPTER 2. LITERATURE REVIEW

The difficulties that have been encountered in the study of Rayleigh-Bénard instabilities parallel those of two of the most intractable problems in fluid mechanics: hydrodynamic stability and the numerical modeling of turbulent flow. Despite the presence of only a single driving force, the nonlinear nature of Rayleigh-Bénard convection gives it a complex and often "chaotic" behavior that is difficult to describe and predict (e.g., Bergé et al., 1984). While the determination of instabilities in buoyancy-driven flows is intrinsically of interest because of the presence of Rayleigh-Bénard convection in a number of important industrial and natural processes, the phenomenon has lately attracted more attention because the relative simplicity of the system lends itself to the study of the mechanisms involved in the transition to turbulence (e.g., Gleick, 1988).

The development of mathematical tools for the study of Rayleigh-Bénard convection has not kept pace with the refinement of experimental efforts. Present numerical methods for solving the governing system of partial differential equations cannot adequately define the whole range of flow regimes and transitions (e.g., Tritton, 1988). In the field of nonlinear dynamics, methods for the study of mathematical stability have seen rapid growth in the past three decades but

are still undergoing development and refinement. Consequently, studies in Rayleigh-Bénard convection have been marked by the continued use of experimental studies to verify the theoretical approaches (e.g., Tritton, 1988).

Bénard (1900, 1901) was the first to conduct rigorous experiments on the problem of buoyancy-driven instabilities in a thin layer of spermaceti heated from below in a gravitational field. At the free surface of the fluid he observed a number of hexagonal convection cells with flow rising in the center of the cell and falling at the perimeter. It was found later by Block (1956) and Pearson (1958) that the cause of these cells was not vertical differences in buoyancy in the fluid layer, but inherently destabilizing surface tension gradients caused by surface temperature variations.

From the theoretical standpoint, the first useful simplification of the equations governing buoyancy-induced flows in a thin fluid layer, the Boussinesq system, was not completely formulated until the turn of the century by Boussinesq (1903). Boussinesq reasoned that for a small vertical temperature gradient, density variations were significant only in the buoyancy term of the Navier-Stokes equations.

Lord Rayleigh (1916) assumed that the flow in Bénard's experiment was buoyancy-induced. He used a fluid layer thin enough to ignore the effect of the sidewalls on the flow

pattern. He performed a linear stability analysis on the Boussinesq system. Linear stability theory allows determination of the first critical Rayleigh number as well as the wavelength of the destabilizing perturbation, but it does not allow determination of the flow patterns of the velocity field (e.g., Knuteson, 1989). Subsequent investigations have refined considerably the linear stability of fluid layers of infinite lateral extent (e.g., Chandrasekhar, 1961).

Experimental work by Koschmieder (1966, 1967, 1969) showed that the side wall of the fluid container does indeed exert an influence on the convective pattern of the flow. For small vertical temperature gradients and certain values of the aspect ratio, the velocity field takes the form of convective roll cells in the shape of the surrounding side walls. In a cylindrical container under such conditions, he found axisymmetric rolls. Theoretical studies by Davis (1968) and Segel (1969) using large but confined geometries obtained the flow fields found in these experiments for rectangular box-shaped containers.

The effect of the Prandtl number on flow regime transitions was investigated in exhaustive experimental studies by Krishnamurti (1970a, 1970b, 1973). She found that flow regime transitions become increasingly more sensitive to variations in the Rayleigh number for fluids with Prandtl numbers approaching zero. In mercury, for example, with a

Prandtl number of 0.025, only turbulent flows are observed after the transition from conduction (e.g., Tritton, 1988).

Until the refinement of certain spectral methods of flow representation (Orszag, 1971a,b), the theoretical study of Rayleigh-Bénard convection in cylindrical geometries was confined to the case of a side wall under "slip" conditions (e.g., Pellew and Southwell, 1940; Zierep, 1963; Ostrach and Pnueli, 1963; Liang et al., 1969). Zierep found that a no-slip side wall did not allow separation of variables. Orszag was able to develop flow representations using expressions other than Fourier series that allowed a rigid no-slip side wall and more realistic flow representation (Orszag, 1971a,b). Charlson and Sani (1970) used a linearized Boussinesq system and a Rayleigh-Ritz method with Bessel function flow representation to find the first three critical Rayleigh numbers for axisymmetric flow. They considered both conducting and insulated side walls. Experimental work by Müller et al. (1984) with liquid gallium compared fairly well with their first critical Rayleigh number results.

A straightforward numerical solution to the Boussinesq system of equations is possible using a number of techniques. There are two tasks that an efficient method must accomplish. The first is to efficiently model the whole range of flow regimes with high resolution on the route to turbulence. This flow modeling is complicated by the difficulty of representing

the dissimilar flow patterns and ever increasing modes of the flow on the route to turbulence. Tarman (1989) used two finite Fourier series of 106 and 297 terms to model turbulent Rayleigh-Bénard convection in a three-dimensional box of infinite horizontal extent and still was not able to accurately model vertical vorticity. Computational efficiency and rapid convergence are therefore paramount. Secondly, it is desirable to be able to detect flow regime transitions easily and precisely. Obtaining an efficient representation of the dependent variables temperature and velocity that can be varied easily with changes in other parameters such as the Rayleigh number to determine stability is difficult.

Finite difference (e.g., Müller et al., 1984), finite element (e.g., Carlson et al., 1985), and spectral methods (e.g., Canuto et al., 1988) are possible numerical approaches to Rayleigh-Bénard convection that can satisfy these conditions. Their application depends upon the particular characteristics of the problem under consideration. The presence and type of nonlinearities is often a deciding factor (e.g., Canuto et al., 1988). The primary difference between the finite difference and finite element methods versus the spectral methods is that the former divide the domain into a grid and solve the system for local grid points or elements, whereas the latter use global expressions to represent the dependent variables (e.g., Canuto et al., 1988).

To determine the instabilities, one approach is to mimic the sensitivity approach of the experimental methods. As the Rayleigh number is gradually increased, instabilities appear as distinct qualitative changes in the flow pattern solutions (e.g., Deane and Sirovich, 1990; Le Queré and Alziary de Rochefort, 1986). For computationally intensive models, this technique is tedious, as it necessitates implementation of the computational procedure with each new value of the Rayleigh number. This approach can also be complicated by the necessity to use long evolutions of the flow to avoid mistaking transient or intermittent flows for the true transitional flow. However, it may be the best approach to determining stability if the transformed systems of the spectral methods are difficult to analyze for stability.

The use of Chebyshev functions to model flows began with Orszag (1971a,b). He found it was possible to use Chebyshev series to model rigid side walls. In addition, he found that Chebyshev representations of dependent variables were suited to many hydrodynamic stability problems because of the accuracy and conciseness of Chebyshev approximations and their infinite-order accuracy compared to finite difference approximations. He used Fast Fourier Transforms to transfer between the physical and spectral spaces (1971b). There have been a number of studies of convection to use Chebyshev series to model two-dimensional and three-dimensional flows.

Haldenwang (1986) found that Chebyshev spectral methods were suitable to modeling dissipation in a convective boundary layer at high Rayleigh numbers. Le Queré and Alziary de Rochefort (1986) found the rapid convergence properties of Chebyshev functions to be advantageous in the problem of Rayleigh-Bénard convection in a square cavity. Some difficulties that are encountered in these Chebyshev spectral flow representation techniques are the necessity of using an implicit or semi-implicit evaluation of the diffusive terms in the Navier-Stokes equation and the lack of natural boundary conditions for the pressure (Le Queré and Alziary de Rochefort, 1986).

If the nonlinearities of the system are no more than quadratic, as they are in the Boussinesq system, then one efficient technique may be to use a Galerkin spectral method (Canuto et al., 1988). This approach transforms the Boussinesq system into a low-order system of ordinary differential equations. A stability analysis can then be used to determine the instabilities of this transformed system. The stability analysis of the dynamical system that results is a theory unto itself (e.g., Wiggins, 1990). The problem arises that a very complex nonlinear analysis may be necessary, one more difficult than the sensitivity approach of the other methods.

For the present study, with its aim of determining only

the first transition to a relatively simple and approximately known laminar flow, a Galerkin method is well-suited to the problem. It is possible to represent the flow and the nonperiodic boundary conditions concisely. A local stability analysis is sufficient to determine the first critical Rayleigh number. The transformed system consists of only three equations, so that the eigenvalue equation is a cubic and the solution will be exact.

The present study parallels the classic nonlinear dynamic analysis of Lorenz (1963). Lorenz used a shorter form of the Fourier Galerkin spectral method representation of Saltzman (1962) to analyze the stability of Rayleigh-Bénard convection cells in the atmosphere. He considered periodic boundary conditions in a two-dimensional Cartesian framework and an infinite lateral extent. He discovered a rich behavior in the resulting low-order system of ordinary differential equations. His model was not extensive enough to accurately represent the whole range of actual flow regimes and Rayleigh instabilities (Nese, 1987), but it gave impetus to the study of "chaos," the stability of nonlinear dynamical systems (e.g., Gleick, 1987).

In the present work, the use of Chebyshev series in cylindrical coordinates to model the flow variables allows the imposition of a rigid, no-slip side wall in the cylindrical container. A Galerkin method is then used to transform the governing system of nonlinear partial differential equations

into a system of first-order nonlinear ordinary differential equations. A local stability analysis of the transformed system similar to that of Gelaro (1987) is used to determine the first critical Rayleigh number.

### **CHAPTER 3. RAYLEIGH-BENARD CONVECTION**

The growth of a crystal from the melt is a solidification process governed by the two heat transfer mechanisms in fluids, conduction and convection. The particular form of heat transfer depends upon the strength of the temperature gradient. As the temperature gradient is gradually raised from an initial zero value, the melt transfers heat by conduction and then by successively more vigorous forms of Rayleigh-Bénard convection--laminar, periodic, quasiperiodic, and turbulent. A useful mathematical model must accurately represent both the physical complexity of each flow field as well as the onset of the transitions between them.

#### **3.1 The Physics of Rayleigh-Bénard Convection**

Rayleigh-Bénard convection is flow that is driven by buoyancy gradients in the fluid. As an illustration of the basic physical mechanism of this type of convection, consider a column of fluid heated from below in a gravitational field (Fig. 6). The higher temperatures near the bottom cause the fluid there to expand, decreasing its density relative to the colder, more dense fluid above it. In this unstable equilibrium, the bottom fluid tends to rise and the top fluid

to fall relative to each other. Motion is initiated only if the driving temperature gradient is high enough to overcome the forces opposing motion. These forces are the frictional effect of the fluid viscosity and the damping effect of thermal conductivity, the tendency of the fluid to transfer heat by conduction rather than by convection. The direction of the flow rotation is determined by the initial conditions (Liang et al., 1969). If flow is initiated, the flow is horizontal at the top and bottom in order to satisfy continuity. The laminar convective flow pattern that is formed is a roll cell or Bénard cell.

The simplest physical configuration illustrating the mechanisms of Rayleigh-Benard convection in the crystal melt consists of a layer of fluid between two extensive horizontal plates in a gravitational field (Fig. 7). Consider that the temperature of the bottom plate  $T_2$  is higher than the temperature of the top plate  $T_1$ ,  $T_2 > T_1$  (Fig. 7). For the conductive case the resulting temperature profile is linear. The ratio  $h/L \ll 1$  so that there is no significant friction at the vertical boundaries and no influence of the sidewall on the flow pattern.

Consider a temperature gradient that is marginally supercritical, sufficient to produce laminar convective flow from the conductive regime. Both conductive and convective heat transfer mechanisms are present in this flow, although

the latter is dominant. At the bottom of the fluid layer, heat from the bottom plate is transferred to the adjacent fluid by conduction. The increased buoyancy of this fluid, caused by the local decrease in its density, induces it to rise. Convective flow then transfers the heat to the vicinity of the top plate, where it is transferred from the fluid to the top plate again by conduction. The fluid, having lost much of its heat, falls and is heated on its way down. When it reaches the vicinity of the lower plate the whole process is repeated.

The linear temperature gradient typical of conduction is modified by convection (Fig. 7). The temperature in the convective region tends to a uniform temperature distribution, cooler fluid at the top being heated, warmer fluid at the bottom being cooled. The more turbulent the flow, the more uniform the temperature distribution tends to be in this region (e.g., Tarman, 1989). Temperature gradients in the conductive regions at the top and bottom boundaries are steep.

For the marginally supercritical temperature gradients typical of laminar convective flow, the number of parallel rolls that are formed in such a thin fluid layer depends upon the aspect ratio of the fluid container. The vertical dimension of these single rolls is determined by the scale of the height of the fluid layer,  $h$  (Shirer, 1987) (Fig. 7). This vertical dimensioning is valid even for containers with

$h/L > 1$  (e.g., Tritton, 1988) (Fig. 6). For a marginally supercritical temperature gradient, a single convection cell will be present in a cylinder with  $h/L > 1$  (e.g., Müller et al., 1984).

Although the flow field may become more complex with increasing temperature gradient, these basic heat transfer mechanisms of conduction at the boundaries and some form of convection in the middle remain valid. The flow fields for the other flow regimes are not so simple, but they can be thought of as superpositions of many different modes of this basic flow.

### 3.2 The Boussinesq System

The system of equations governing Rayleigh-Bénard convection consists of the continuity (conservation of mass), conservation of energy, and Navier-Stokes (conservation of linear momentum) equations. In cylindrical coordinates, these equations are:

$$\frac{\partial \rho}{\partial t} + \nabla \cdot (\rho \mathbf{v}) = 0 \quad (3.1)$$

$$\rho \hat{C}_v \frac{DT}{Dt} = -(\nabla \cdot \mathbf{q}) - T \left( \frac{\partial p}{\partial T} \right)_\rho (\nabla \cdot \mathbf{v}) - (\boldsymbol{\tau} : \nabla \mathbf{v}) \quad (3.2)$$

$$\rho \left( \frac{\partial v_r}{\partial t} + v_r \frac{\partial v_r}{\partial r} + \frac{v_\theta}{r} \frac{\partial v_r}{\partial \theta} - \frac{v_\theta^2}{r} + v_z \frac{\partial v_r}{\partial z} \right) = - \frac{\partial p}{\partial r} -$$

$$\left( \frac{1}{r} \frac{\partial}{\partial r} (r \tau_{rr}) + \frac{1}{r} \frac{\partial \tau_{r\theta}}{\partial \theta} - \frac{\tau_{\theta\theta}}{r} + \frac{\partial \tau_{rz}}{\partial z} \right) + \rho g_r \quad (3.3a)$$

$$\rho \left( \frac{\partial v_\theta}{\partial t} + v_r \frac{\partial v_\theta}{\partial r} + \frac{v_\theta}{r} \frac{\partial v_\theta}{\partial \theta} + \frac{v_r v_\theta}{r} + v_z \frac{\partial v_\theta}{\partial z} \right) = - \frac{1}{r} \frac{\partial p}{\partial \theta} -$$

$$\left( \frac{1}{r^2} \frac{\partial}{\partial r} (r^2 \tau_{r\theta}) + \frac{1}{r} \frac{\partial \tau_{\theta\theta}}{\partial \theta} + \frac{\partial \tau_{\theta z}}{\partial z} \right) + \rho g_\theta \quad (3.3b)$$

$$\rho \left( \frac{\partial v_z}{\partial t} + v_r \frac{\partial v_z}{\partial r} + \frac{v_\theta}{r} \frac{\partial v_z}{\partial \theta} + v_z \frac{\partial v_z}{\partial z} \right) = - \frac{\partial p}{\partial z} -$$

$$\left( \frac{1}{r} \frac{\partial}{\partial r} (r \tau_{rz}) + \frac{1}{r} \frac{\partial \tau_{\theta z}}{\partial \theta} + \frac{\partial \tau_{zz}}{\partial z} \right) + \rho g_z \quad (3.3c)$$

where

$$\tau_{rr} = -\mu \left[ 2 \frac{\partial v_r}{\partial r} - \frac{2}{3} (\nabla \cdot \mathbf{v}) \right] \quad (3.4a)$$

$$\tau_{\theta\theta} = -\mu \left[ 2 \left( \frac{1}{r} \frac{\partial v_\theta}{\partial \theta} + \frac{v_r}{r} \right) - \frac{2}{3} (\nabla \cdot \mathbf{v}) \right] \quad (3.4b)$$

$$\tau_{zz} = -\mu \left[ 2 \frac{\partial v_z}{\partial z} - \frac{2}{3} (\nabla \cdot \mathbf{v}) \right] \quad (3.4c)$$

$$\tau_{r\theta} = \tau_{\theta r} = -\mu \left[ r \frac{\partial}{\partial r} \left( \frac{v_\theta}{r} \right) + \frac{1}{r} \frac{\partial v_r}{\partial \theta} \right] \quad (3.4d)$$

$$\tau_{\theta z} = \tau_{z\theta} = -\mu \left[ \frac{\partial v_{\theta}}{\partial z} + \frac{1}{r} \frac{\partial v_z}{\partial \theta} \right] \quad (3.4e)$$

$$\tau_{zr} = \tau_{rz} = -\mu \left[ \frac{\partial v_z}{\partial r} + \frac{\partial v_r}{\partial z} \right] \quad (3.4f)$$

where

$C_v$  = heat capacity at constant volume, per unit mass

$(g_r, g_{\theta}, g_z)$  = acceleration of gravity

$p$  = pressure

$\mathbf{q}$  = energy flux relative to mass average velocity

$T$  = absolute temperature

$t$  = time

$\mathbf{v}$  = velocity vector =  $(v_r, v_{\theta}, v_z)$

$\mu$  = dynamic viscosity

$\rho$  = fluid density

$\tau$  = viscous stress tensor

$\tau_{ij}$  = viscous stress tensor component

$( )_v$  = per unit volume

$( : )$  = scalar product of tensors

This system is solved for the dependent variables  $\mathbf{v}$ ,  $p$ , and  $T$  in order to determine the velocity, pressure, and temperature fields.

This system of three partial differential equations is nonlinear and coupled and is consequently difficult to solve numerically. The system can be simplified for buoyancy-driven convection under certain conditions to the Boussinesq system (Boussinesq, 1903). The derivation is based on the assumption that for a small temperature gradient in the fluid layer, the

variation in the density is small but sufficient to cause flow due to buoyancy differences (e.g., Drazin and Reid, 1981). The density is assumed to be constant except in the buoyancy term  $\rho g_z$  of Navier-Stokes equation 3.3c, where the density is assumed to vary as a linear function of the temperature,

$$\Delta\rho = -\alpha\rho_0\Delta T \quad (3.5)$$

where

$\rho$  = fluid density  
 $\rho_0$  = reference density  
 $\alpha$  = coefficient of thermal expansion of the fluid  
 $\Delta T$  = temperature difference in the fluid layer

Other assumptions that are made in the derivation are (e.g., Knuteson, 1989):

1. Gravity is the only external force and is directed downwards.
2. Accelerations in the fluid are small compared with  $g$ .
3. All physical properties of the fluid are constant
4. There is no internal heat generation.

All these assumptions are satisfied in the system considered here.

Rayleigh-Bénard convective flow in a low-Prandtl number crystal melt in the Bridgman configuration is therefore governed by the Boussinesq system with the following specific

conditions: a cylindrical geometry, no-slip conditions at all surfaces, conducting top and bottom, an insulated side wall, and a planar surface at the crystal interface. In three-dimensional cylindrical coordinates, the nondimensional form of the Boussinesq equations (continuity, conservation of energy, and Navier-Stokes) is (e.g., Knuteson, 1989):

$$\nabla \cdot \mathbf{v}^* = 0 \quad (3.6)$$

$$\frac{\partial T^*}{\partial t^*} + \mathbf{v}^* \cdot \nabla T^* = \nabla^2 T^* \quad (3.7)$$

$$\frac{1}{Pr} \left( \frac{\partial \mathbf{v}^*}{\partial t^*} + \mathbf{v}^* \cdot \nabla \mathbf{v}^* \right) = -\nabla p^* + \nabla^2 \mathbf{v}^* + Ra T^* \hat{e}_z \quad (3.8)$$

where

$\hat{e}_z$ , unit vector in the z-direction  
 $g$ , acceleration of gravity  
 $h$ , height of the cylinder  
 $p^*(r^*, \theta, z^*, t^*)$ , pressure

$Pr$ , Prandtl number =  $\frac{\nu}{\kappa}$

$R$ , radius of cylinder  
 $r^*$ , nondimensional radial coordinate

$Ra$ , Rayleigh number =  $\frac{g\alpha\Delta T h^3}{\nu\kappa}$

$T^*(r^*, \theta, z^*, t^*)$ , temperature  
 $T_2$ , temperature at the bottom boundary  
 $T_1$ , temperature at the top boundary  
 $\Delta T$ , temperature difference in the fluid layer =  $T_2 - T_1$   
 $\mathbf{v}^*(r^*, \theta, z^*, t^*)$ , velocity vector  
 $z^*$ , nondimensional vertical coordinate

$\alpha$ , volumetric thermal expansion coefficient  
 $\gamma$ , aspect ratio =  $h/R$   
 $\theta$ , angular coordinate

$\kappa$ , thermal diffusivity  
 $\nu$ , kinematic viscosity

$0 \leq r^* \leq 1$ ,  $0 \leq \theta \leq 2\pi$ ,  $-\gamma/2 \leq z^* \leq \gamma/2$  cylindrical coordinate system

For the nondimensionalization, velocities are scaled with  $\kappa/h$ , temperature with  $\Delta T$ , pressure with  $\rho \kappa^2/h^2$ , time with  $h^2/\kappa$ , and lengths with the height of the fluid column,  $h$ :

$$v^* = \frac{vh}{\kappa} \quad (3.9a)$$

$$T^* = \frac{T - T_2}{\Delta T} \quad (3.9b)$$

$$p^* = \frac{ph^2}{\rho \kappa^2} \quad (3.9c)$$

$$r^* = \frac{r}{h} \quad (3.9d)$$

$$t^* = \frac{t\kappa}{h^2} \quad (3.9e)$$

$$z^* = \frac{z}{h} \quad (3.9f)$$

For this particular problem, with the radius of the cylinder equal to its height, the aspect ratio  $\gamma$  is one. The velocities are zero at the rigid, no-slip boundaries:

$$\begin{aligned} v^*(1, \theta, z^*, t^*) &= v^*(r^*, \theta, -\gamma/2, t^*) = v^*(r^*, \theta, \gamma/2, t^*) \\ &= 0 \end{aligned} \quad (3.10)$$

The top and bottom faces are conducting surfaces and are at constant temperature:

$$T^*(r^*, \theta, \gamma/2, t^*) = C_1, \quad C_1 \in \mathbb{R}, \quad C_1 > 0^\circ K \quad (3.11a)$$

$$T^*(r^*, \theta, -\gamma/2, t^*) = C_2, \quad C_2 \in \mathbb{R}, \quad C_2 > 0^\circ K \quad (3.11b)$$

For the side wall, two cases are considered, insulated

$$\frac{\partial T^*}{\partial r^*}(1, \theta, z^*, t^*) = 0 \quad (3.12)$$

or conducting surfaces:

$$T^*(1, \theta, z^*, t^*) = C, \quad C \in \mathbb{R}, \quad C > 0^\circ K \quad (3.13)$$

It is evident from equations 3.6-3.8 that dynamic similarity is attained by using the nondimensional parameters  $Ra$  and  $Pr$ . It is not possible to use the Reynolds number for dynamic similarity because of the absence of a characteristic velocity in the conductive regime.

The Rayleigh number is a relative measure of the forcing mechanisms that drive Rayleigh-Bénard convection and the opposing mechanisms that damp the flow. The buoyancy differences in the fluid layer that create the thermal instability are the result of density variations. These variations are caused by the temperature difference  $\Delta T$  and the consequent thermal expansion of the fluid, indicated by  $\alpha$ . The height of the fluid layer  $h$  is included in the formulation because it is essentially the temperature gradient that is the forcing mechanism. Two effects inhibit convective flow, the viscosity  $\nu$ , the resistance of the fluid to shear deformation, and the thermal diffusivity  $\kappa$ , the tendency of the thermal

conductivity of the fluid to transfer heat by conduction rather and thus postpone the onset of convection.

The Prandtl number, a property of the fluid, indicates the relative molecular transport rates of momentum versus heat. It is evident from the Navier-Stokes equations (eqs. 3.3-3.4) that a low Prandtl number significantly amplifies the role of the inertial nonlinearity (e.g., Knuteson, 1989). This effect is felt from the initiation of laminar convection.

The aspect ratio  $\gamma$  indicates the relative size of the container. It is one factor that determines the number and size of the convection cells in the container. For laminar convection in the cylinder of aspect ratio one, only one concentric roll is anticipated (Fig. 8).

The Boussinesq system has no direct analytical solution. Numerical solutions are approximations of the true solution, and for this reason they are not able to accurately describe or predict the full range of flow patterns of the fluid (e.g., Tritton, 1988). In addition, the theory of stability of systems of partial differential equations is incomplete. Determination of the stability of the Boussinesq system must be approached indirectly, either by transforming to an approximate system of ordinary differential equations that is amenable to stability analysis or by a parametric study to detect qualitative changes in the flow or temperature fields.

In the present study the former approach is taken. A

relatively simple flow is approximated using finite Chebyshev series. A Galerkin spectral method is used to transform the Boussinesq system into a first-order system of three ordinary differential equations. A local stability analysis is then performed to determine the first critical Rayleigh number.

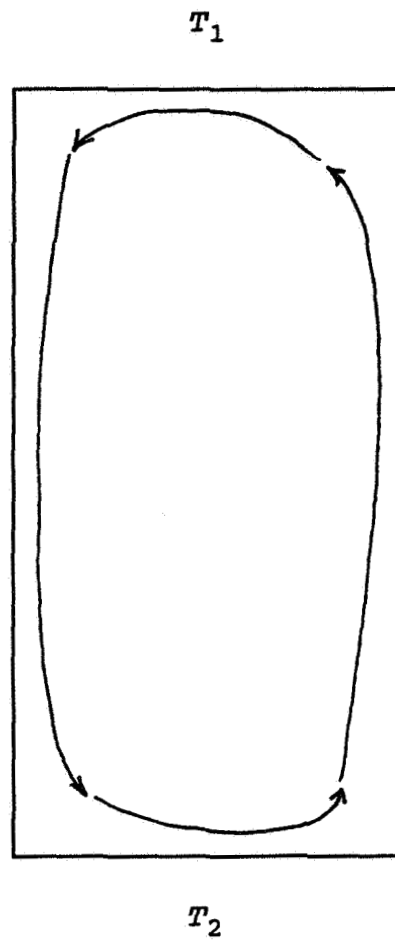


**Figure 6.** Rayleigh-Bénard convection in a fluid column.

$$T_2 > T_1.$$

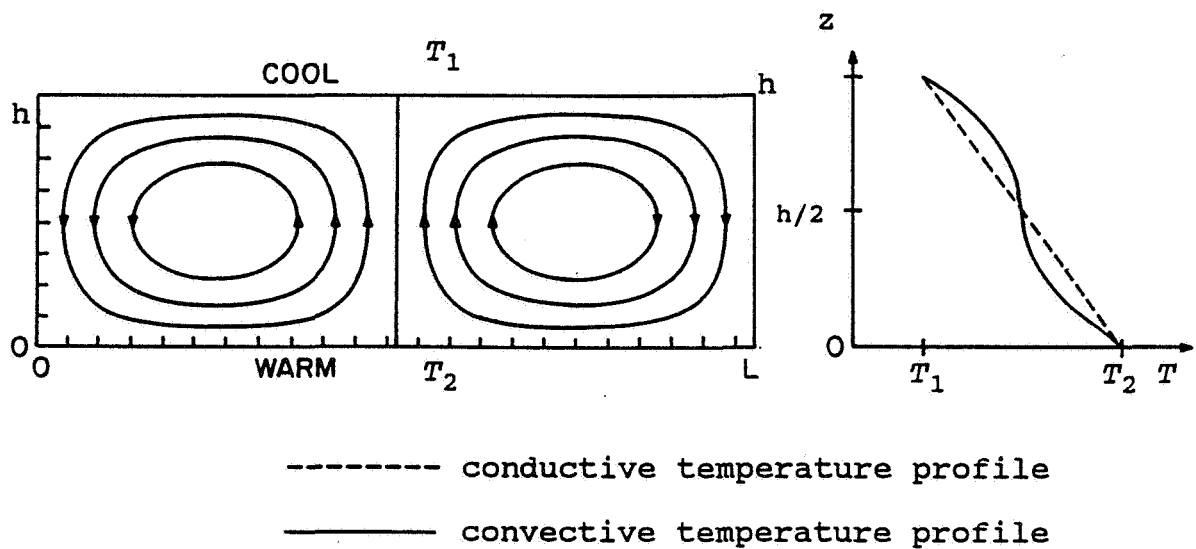


**Figure 7.** Parallel laminar convection rolls in a closed rectangular box with slip side walls. The convective redistribution of heat is evident from the temperature gradients in the fluid layer (from Shirer, 1987).

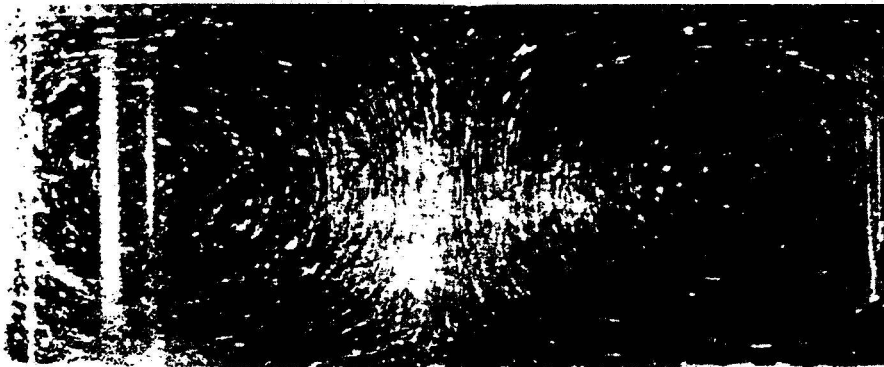


**Figure 8.** Axisymmetric convection roll in cylinder of aspect ratio one (from Müller et al., 1984).

#### CHAPTER 4. THE CHEBYSHEV-GALERKIN SPECTRAL METHOD

Galerkin spectral methods transform a system of partial differential equations into a low-order system of ordinary differential equations, a form more amenable to solution as well as to stability analysis. A Chebyshev-Galerkin spectral method is especially useful for modeling nonperiodic laminar flows in simple geometries (Orszag, 1971b). Many such flows can be approximated by continuous polynomial functions, and because Chebyshev functions are essentially polynomials, dependent variables can be represented by finite series of Chebyshev functions. A Galerkin method employing Fourier series, although much easier to apply in such cases, would not allow accurate modeling of the nonperiodic flows and boundary conditions. The set of Chebyshev functions is also a member of a class of functions having the orthogonality properties necessary to implement the Galerkin method.

The laminar axisymmetric flow of a low-Prandtl number liquid metal in a rigid, closed cylindrical container of equal height and radius is a case of a relatively simple nonperiodic flow with nonperiodic boundary conditions. The convection cell has a toroidal shape that is assumed to be symmetric about the horizontal mid-plane (Fig. 9). Although the convergence of flows at the center of the cylinder displaces the rotational center of the cell outward to a point past  $R/2$

(Müller et al., 1984)), both velocity and temperature with their boundary conditions can be represented fairly accurately by continuous polynomials and therefore by Chebyshev series.

The physical transition of the fluid from the conductive to the convective regime can be approached mathematically as a perturbation problem. The laminar convection state is treated as a perturbation of the basic conductive state. Analysis of the growth of the convective perturbation indicates the critical point of transition between the two regimes.

The axisymmetric Boussinesq system is first perturbed. It is then simplified by transforming the Navier-Stokes equation into a vorticity equation and introducing a Stokes stream function to reduce the number of dependent variables. A Chebyshev-Galerkin method is then applied to the resulting system of equations. Dependent variable Chebyshev series consisting of terms with separated variable expressions for time and the two spatial directions are substituted into the Boussinesq system. An ordinary differential equation of first order for each of the time-varying coefficients is obtained by multiplying a partial differential equation by the orthogonal test function of the desired time-dependent coefficient and integrating over the domain. Once the partial differential Boussinesq system has been transformed into a low-order system

of ordinary differential equations, the stability analysis can be performed.

#### **4.1 Perturbation of the Boussinesq System**

Perturbation of the Boussinesq system is useful because it allows the system to be expressed in terms of the convective flow variables. Normally, a perturbation analysis for a strongly nonlinear equation like the Navier-Stokes equation is not straightforward. However, in this case, the zero velocity field of the conductive flow field allows nonlinear terms to be retained in the first order equations.

The nondimensional cylindrical Boussinesq system from Chapter 3,

$$\nabla \cdot \mathbf{v}^* = 0 \quad (4.1)$$

$$\frac{\partial T^*}{\partial t^*} + \mathbf{v}^* \cdot \nabla T^* = \nabla^2 T^* \quad (4.2)$$

$$\frac{1}{Pr} \left( \frac{\partial \mathbf{v}^*}{\partial t^*} + \mathbf{v}^* \cdot \nabla \mathbf{v}^* \right) = -\nabla p^* + \nabla^2 \mathbf{v}^* + Ra T^* \hat{e}_z \quad (4.3)$$

is used here. Assuming axisymmetric flow, the above system of equations can be simplified by considering the following properties of this flow, which hold by definition:

$$v_{\theta}^*(r^*, \theta, z^*, t^*) = 0 \quad (4.4)$$

$$\frac{\partial(\ )}{\partial \theta} = 0 \quad (4.5)$$

The first step in the perturbation procedure is to perturb the dependent variables velocity, pressure, and temperature. These variables are expressed as the sum of a basic state, conduction (0-subscript terms), and a small convective perturbation of this basic state (primed terms):

$$v^*(r^*, z^*, t^*) = v_0^* + v'^*(r^*, z^*, t^*) \quad (4.6)$$

$$p^*(r^*, z^*, t^*) = p_0^*(z^*) + p'^*(r^*, z^*, t^*) \quad (4.7)$$

$$T^*(r^*, z^*, t^*) = T_0^*(z^*) + T'^*(r^*, z^*, t^*) \quad (4.8)$$

In the conductive state, the velocity vector is zero, the temperature variation is linear, and the pressure gradient is hydrostatic:

$$v_0^* = 0 \quad (4.9)$$

$$p_0^*(z^*) = p_2^* - (g h^3 / \kappa^2) (z^* + 1/2) \quad (4.10)$$

$$T_0^*(z^*) = T_2^* - (z^* + 1/2) \quad (4.11)$$

The terms  $p_2^*$  and  $T_2^*$  are the pressure and temperature, respectively, at the bottom of the cylinder.

Convective flow occurs if the perturbations are not damped over time. In that case, the perturbation variables represent the convective flow field.

The expressions for  $v^*$ ,  $p^*$ , and  $T^*$  are substituted into the Boussinesq system. After some algebraic manipulations and

deletion of primes and asterisks, the system for the perturbed variables becomes:

$$\nabla \cdot \mathbf{v} = 0 \quad (4.12)$$

$$\frac{\partial T}{\partial t} + \mathbf{v} \cdot \nabla T - v_z = \nabla^2 T \quad (4.13)$$

$$\frac{1}{\text{Pr}} \left( \frac{\partial \mathbf{v}}{\partial t} + \mathbf{v} \cdot \nabla \mathbf{v} \right) = -\nabla p_0 - \nabla p + \nabla^2 \mathbf{v} + (\text{Ra } T_0 + \text{Ra } T) \hat{\mathbf{e}}_z \quad (4.14)$$

Note the retention of the nonlinearities in the Navier-Stokes and energy equations. In this perturbed Boussinesq system as in the unperturbed, it is again apparent that a low Prandtl number exerts a significant nonlinear effect due to the inertial term

$$\frac{1}{\text{Pr}} \mathbf{v} \cdot \nabla \mathbf{v} \quad (4.15)$$

This effect becomes important as soon as convection is initiated. In any flow regime with nonzero finite velocity vectors, the Navier-Stokes equations for low-Prandtl number fluids are highly nonlinear (e.g., Knuteson, 1989).

#### **4.2 Simplification of the Perturbed Boussinesq System**

The stability analysis of the perturbed Boussinesq system involves the solution of a variational equation that is a

polynomial. The degree of this equation can be decreased and its solution facilitated by reducing the number of dependent variables in the perturbed Boussinesq system. In addition to decreasing the size of the resulting system of ordinary differential equations, this simplification also eliminates the need to determine the pressure.

Both pressure gradient terms  $-\nabla p_0$  and  $-\nabla p'$  as well as the conductive buoyancy term  $RaT_0\hat{e}_z$  in the perturbed Navier-Stokes equation can be eliminated by taking the curl of the equation and thereby transforming it into a vorticity equation:

$$\frac{1}{Pr} \left[ \nabla \times \left( \frac{\partial \mathbf{v}}{\partial t} + \mathbf{v} \nabla \mathbf{v} \right) \right] = \nabla \times (\nabla^2 \mathbf{v} + Ra T \hat{e}_z) \quad (4.16)$$

A nondimensional Stokes stream function  $\psi$  is introduced to reduce the number of dependent variables from three  $(v_r, v_z, T)$  to two  $(\psi, T)$ . The  $\psi$  is made nondimensional by scaling it with the thermal diffusivity,  $\kappa$ , and the height of the cylinder,  $h$ . The nondimensional radial and vertical velocities  $v_r$  and  $v_z$  may then be expressed in terms of  $\psi$ :

$$v_r = -\frac{1}{r} \frac{\partial \psi}{\partial z} \quad (4.17)$$

$$v_z = \frac{1}{r} \frac{\partial \psi}{\partial r} \quad (4.18)$$

Because this stream function satisfies the continuity equation exactly,

$$\nabla \cdot \mathbf{v} = \frac{1}{r} \frac{\partial(r v_r)}{\partial r} + \frac{\partial v_z}{\partial z} \quad (4.19a)$$

$$= \frac{1}{r} \frac{\partial}{\partial r} \left[ r \left( -\frac{1}{r} \frac{\partial \psi}{\partial z} \right) \right] + \frac{\partial}{\partial z} \left( \frac{1}{r} \frac{\partial \psi}{\partial r} \right) \quad (4.19b)$$

$$= -\frac{1}{r} \frac{\partial^2 \psi}{\partial r \partial z} + \frac{1}{r} \frac{\partial^2 \psi}{\partial r \partial z} \quad (4.19c)$$

$$= 0, \quad (4.19d)$$

the equation may be dropped, and the perturbed Boussinesq system reduces to a two-equation system in  $\psi$  and  $T$ :

$$\frac{\partial T}{\partial t} + \frac{1}{r} J(\psi, T) - \frac{1}{r} \frac{\partial \psi}{\partial r} = \nabla^2 T \quad (4.20)$$

$$\frac{1}{Pr} \left\{ \nabla \times \left[ \frac{\partial}{\partial t} \left( -\frac{1}{r} \frac{\partial \psi}{\partial z}, \frac{1}{r} \frac{\partial \psi}{\partial r} \right) + \left( -\frac{1}{r} \frac{\partial \psi}{\partial z}, \frac{1}{r} \frac{\partial \psi}{\partial r} \right) \cdot \nabla \left( -\frac{1}{r} \frac{\partial \psi}{\partial z}, \frac{1}{r} \frac{\partial \psi}{\partial r} \right) \right] \right\} =$$

$$\nabla \times \left[ \nabla^2 \left( -\frac{1}{r} \frac{\partial \psi}{\partial z}, \frac{1}{r} \frac{\partial \psi}{\partial r} \right) \right] - Ra \frac{\partial T}{\partial r} \hat{e}_\theta \quad (4.21)$$

in which the Jacobian  $J(f_1, f_2)$  is

$$J(f_1, f_2) = \frac{\partial f_1}{\partial r} \frac{\partial f_2}{\partial z} - \frac{\partial f_1}{\partial z} \frac{\partial f_2}{\partial r} \quad (4.22)$$

This system of two equations in  $\psi$  and  $T$  requires ten boundary conditions for the problem to be well posed. In the energy equation (eq. 4.20), which is second-order in  $T$  in  $r$  and  $z$ , four boundary conditions are necessary to uniquely determine the coefficients of the particular solution for  $T$ , two from the  $r$ -variable and two from the  $z$ -variable. In the

same manner, six boundary conditions are needed for the solution of  $\psi$  in the third-order vorticity equation (eq. 4.21) in  $r$  and  $z$ .

The ten boundary conditions for this problem are based on the model of the cylindrical ampoule used in the Bridgman method as well as one characteristic of axisymmetric flow. The ampoule is considered to have rigid, no-slip surfaces:

$$\frac{\partial \psi}{\partial r}(1, z, t) = \frac{\partial \psi}{\partial r}(r, -\frac{1}{2}, t) = \frac{\partial \psi}{\partial r}(r, \frac{1}{2}, t) = 0 \quad (4.23a)$$

$$\frac{\partial \psi}{\partial z}(1, z, t) = \frac{\partial \psi}{\partial z}(r, -\frac{1}{2}, t) = \frac{\partial \psi}{\partial z}(r, \frac{1}{2}, t) = 0 \quad (4.24b)$$

The radial velocity on the center line of the ampoule is zero:

$$\frac{\partial \psi}{\partial z}(0, z, t) = 0 \quad (4.24)$$

The top and bottom are conducting surfaces. They conduct heat into and out of the fluid at the fluid-surface interface, but they maintain a constant temperature. Mathematically, the temperature perturbation is zero:

$$T(r, -\frac{1}{2}, t) = T(r, \frac{1}{2}, t) = 0 \quad (4.25)$$

For the thermal boundary conditions at the side wall, two cases are considered, in the first case a side wall that is conducting,

$$T(1, z, t) = 0 \quad (4.26)$$

and in the second, a side wall that is insulated and allows no transfer of heat across the interface,

$$\frac{\partial T}{\partial r}(1, z, t) = 0 \quad (4.27)$$

### 4.3 Chebyshev Series Representation of Dependent Variables

In the Chebyshev-Galerkin spectral method, the dependent variables are represented by finite Chebyshev series. A separation of variables approach is used. Each term in the series is the product of two spatially-dependent expressions and a time-dependent amplitude coefficient. Successive terms represent modes of the flow, and the series is truncated when the desired number of modes is represented. The stream function  $\psi$  and the temperature  $T$  in the perturbed Boussinesq system may be represented in the following manner:

$$\psi(r, z, t) = \sum_i \sum_j \psi_{ij}(t) \psi_i(r) \psi_j(z) \quad i, j \in \{0, 1, 2, \dots\} \quad (4.28a)$$

$$= \sum_i \sum_j \psi_{ij}(t) [a_i T_i(r)] [b_j T_j(z)] \quad a_i, b_j \in \mathbb{R} \quad (4.28b)$$

$$T(r, z, t) = \sum_k \sum_l T_{kl}(t) T_k(r) T_l(z) \quad k, l \in \{0, 1, 2, \dots\} \quad (4.29a)$$

$$= \sum_k \sum_l T_{kl}(t) [c_k T_k(r)] [d_l T_l(z)] \quad c_k, d_l \in \mathbb{R} \quad (4.29b)$$

in which the Chebyshev function  $T_n$  is defined by:

$$T_n(x) = \cos(n \arccos x) \quad x \in [-1, 1], \quad n \in \{0, 1, 2, \dots\} \quad (4.30)$$

The stability of a single mode, laminar axisymmetric flow, is being considered in the present study. The relative simplicity of this flow allows the number of terms and the specific coefficients in these Chebyshev series to be determined fairly precisely. This axisymmetric flow can be approximated easily by using Chebyshev functions, to the extent that the spatial coefficients  $a_i$ ,  $b_j$ ,  $c_k$ , and  $d_l$  can be determined. Even though a large number of terms is required to represent this flow, the analysis is simplified by the fact that the presence of a single mode requires that all constituent "submodes" move together. The same temporal coefficient must then be common to all terms. The most significant result of this conciseness of the flow representation is that the stability analysis is greatly simplified.

By way of contrast, a model that investigated the series of flow regime transitions on the route to turbulence would have to incorporate a very large number of terms with

differing temporal coefficients. The coefficients  $a_i$ ,  $b_j$ ,  $c_k$ , and  $d_l$  would not be able to be specified and would be incorporated into the appropriate temporal coefficients. Only in this manner could the model represent the multiplicity of flow regimes as well as account for the increasing number of superimposed modes within each flow regime as it becomes more complex.

The spatial distribution of  $\psi$  in the  $r$  and  $z$  planes is determined by the continuity requirement  $\nabla \cdot \mathbf{v} = 0$  as well as by the boundary conditions for  $v_r$  and  $v_z$ , obtained from the boundary conditions for  $\psi$ . With these constraints, it is possible to represent the entire flow field by a single term for  $\psi$  in the stream function series.

Letting  $\psi$  be the expansion

$$\psi(r, z, t) = \psi(t) \psi(r) \psi(z), \quad (4.31)$$

then by using the Stokes stream function definitions, the distributions of  $v_r$  and  $v_z$  in  $r$  and  $z$  can be represented in terms of their corresponding  $\psi$  distributions:

$$v_r(r, z, t) = -\frac{1}{r} \frac{\partial \psi}{\partial z} \quad (4.32a)$$

$$= -\psi(t) \left[ \frac{1}{r} \psi(r) \right] \left[ \frac{\partial \psi(z)}{\partial z} \right] \quad (4.32b)$$

$$= v_r(t) v_r(r) v_r(z) \quad (4.32c)$$

$$v_z(r, z, t) = \frac{1}{r} \frac{\partial \psi}{\partial r} \quad (4.33a)$$

$$= \psi(t) \left[ \frac{1}{r} \frac{\partial \psi(r)}{\partial r} \right] [\psi(z)] \quad (4.33b)$$

$$= v_z(t) v_z(r) v_z(z) \quad (4.33c)$$

It is possible to approximate the velocity distributions by using polynomials. Use of these direct relations between the velocities and  $\psi$  then allows determination of approximate  $\psi$  spatial terms in Chebyshev series.

For example, examination of the axisymmetric flow field (Fig. 10) reveals that the radial variation in  $v_z(r, z, t)$  for  $r \in [0, 1]$  may be approximated by a cubic polynomial (Fig. 11). This rotational flow is assumed to move downward at the center of the cylinder. This direction of flow is not critical. Four conditions that specify this cubic curve include the velocity boundary conditions:

$$\cdot v_z(1, z, t) = 0 \quad (\text{no-slip condition at side wall}) \quad (4.34)$$

$$\cdot v_r(1, z, t) = 0 \quad (\text{no-penetration condition}) \quad (4.35)$$

$$\cdot \partial v_z / \partial r(0, z, t) = 0 \quad (\text{maximum } v_z \text{ value at center line}) \quad (4.36)$$

$$\cdot v_z(0, z, t) = -1 \quad (\text{arbitrary intercept}) \quad (4.37)$$

The derivation of  $v_r(r)$  depends directly upon  $v_z(r)$ , both being functions of  $\psi$ . The  $v_r$  condition above (eq. 4.35) is necessary to ensure that the form of  $v_z$  allows this condition to be met upon derivation of  $v_r$ .

Letting  $v_z(r)$  be the following general cubic polynomial,

$$v_z(r) = ar^3 + br^2 + cr + d, \quad (4.38)$$

the intercept condition (eq. 4.37) determines  $d = -1$ , and the maximum condition (eq. 4.36) determines  $c = 0$ . Substituting these values, the no-slip condition (eq. 4.34) becomes

$$a + b = 1 \quad (4.39)$$

For the no-penetration boundary condition,  $v_r(r)$  must first be derived, employing the mutual dependence on  $\psi$ . The variation of  $\psi$  in  $r$  is first found by taking the polynomial for  $v_z(r)$  and integrating to solve for  $\psi(r)$ ,

$$v_z(r) = \frac{1}{r} \frac{\partial \psi(r)}{\partial r} \quad (4.40)$$

$$\psi(r) = \int r v_z(r) dr \quad (4.41a)$$

$$= \int r(ar^3 + br^2 - 1)dr \quad (4.41b)$$

$$= \frac{a}{5}r^5 + \frac{b}{4}r^4 - \frac{1}{2}r^2 + e \quad (4.41c)$$

The variation in  $r$  for  $v_r$  then becomes (Fig. 12):

$$v_r(r) = \frac{1}{r} \psi(r) \quad (4.42a)$$

$$= \frac{a}{5}r^4 + \frac{b}{4}r^3 - \frac{1}{2}r + \frac{e}{r} \quad (4.42b)$$

The constant of integration "e" must be zero in order for  $v_r(r)$  to be defined at  $r = 0$ . The no-penetration condition then becomes:

$$\frac{a}{5} + \frac{b}{4} = 0 \quad (4.43)$$

Solving for the coefficients a and b using the above equation 4.43 and equation 4.39,  $a = -5$  and  $b = 6$ . The equation for  $v_z(r)$  becomes (Fig. 11):

$$v_z(r) = -5r^3 + 6r^2 - 1 \quad (4.44)$$

This curve models the salient physical features of the flow. The change in sign of the vertical velocity in this closed container indicates flow rotation. The location of the r-intercept to the right of  $r = R/2$  as well as the relative magnitudes of the maximum and minimum on the interval show the flow convergence at the center. The flow profile at the wall takes the approximate shape of a boundary layer.

The equation for  $v_r(r)$  is (Fig. 12):

$$v_r(r) = -r^4 + \frac{3}{2}r^3 - \frac{1}{2}r \quad (4.45)$$

The radial velocity  $v_z$  is zero at  $r = 0$ , and the profile near the center is similar to that of a boundary layer.

The equation for  $\psi(r)$  is:

$$\psi(r) = -r^5 + \frac{3}{2}r^4 - \frac{1}{2}r^2 \quad (4.46)$$

For the purposes of the Galerkin method,  $\psi(r)$  may be expressed in Chebyshev form as:

$$\begin{aligned} \psi(r) = & \left[ -\frac{1}{512}T_5(2r-1) - \frac{1}{128}T_4(2r-1) + \frac{3}{512}T_3(2r-1) + \right. \\ & \left. \frac{1}{32}T_2(2r-1) - \frac{1}{256}T_1(2r-1) - \frac{3}{128}T_0(2r-1) \right] \quad (4.47) \end{aligned}$$

Expressing  $\psi$  in terms of the quantity  $2r-1$  for  $r \in [0,1]$  effectively translates the expression into the domain of all Chebyshev functions,  $[-1,1]$ , and allows the orthogonality of Chebyshev functions to be used to simplify the integration of the equations in a later step.

In a manner similar to the procedure above, the  $\psi(z)$ ,  $v_r(z)$  (Fig. 13), and  $v_z(z)$  (Fig. 14) terms for  $z \in [-\frac{1}{2}, \frac{1}{2}]$  can be determined. Using the relationships in equations 4.32b,c and 4.33b,c the equations for  $v_r(z)$  and  $v_z(z)$  can be related through  $\psi$ :

$$v_r(z) = \frac{\partial \psi(z)}{\partial z} \quad (4.48a)$$

$$= \frac{\partial v_z(z)}{\partial z} \quad (4.48b)$$

The following conditions are used to derive a quartic distribution for  $v_z(z)$  and a cubic distribution for  $v_r(z)$ :

$$v_z(r, \pm \frac{1}{2}, t) = 0 \quad (\text{no-penetration}) \quad (4.49)$$

$$v_r(r, \pm \frac{1}{2}, t) = 0 \quad (\text{no-slip at top and bottom boundaries}) \quad (4.50)$$

$$\partial v_z / \partial z(r, 0, t) = 0 \quad (\text{maximum } v_z \text{ value at midplane}) \quad (4.51)$$

$$v_z(r, 0, t) = 1 \quad (\text{arbitrary intercept}) \quad (4.52)$$

$$\partial v_r / \partial z(r, \pm 0.29, t) = 0 \quad (\text{maximum } v_r \text{ value}) \quad (4.53)$$

The last condition for fixing the height of the maximum radial velocity  $v_r(z)$  allows the thickness of the boundary layers at the top and bottom to be modified. The values of  $z = \pm 0.29$  were chosen to smooth the transition of the maximum  $v_z(z)$  value at  $0.8R$  near the side wall (Fig. 11) to these maximum  $v_r(z)$  values at  $z = \pm 0.21h$ . The  $\pm 0.29$  values also allow integer values of the coefficients.

After some algebra, the following distributions are derived:

$$\psi(z) = 16z^4 - 8z^2 + 1 \quad (4.54a)$$

$$= \left[ \frac{1}{128} T_4(2z) - \frac{7}{32} T_2(2z) + \frac{99}{128} T_0(2z) \right] \quad (4.54b)$$

$$v_r(z) = 64z^3 - 16z \quad (4.55)$$

$$v_z(z) = 16z^4 - 8z^2 + 1 \quad (4.56)$$

Note the antisymmetry of the  $v_r(z)$  curve, the flow moving in towards the center at the top and outward at the bottom.

Combining the two spatial expressions,  $\psi$  becomes:

$$\begin{aligned} \psi(r, z, t) = \psi_{54}(t) & \left[ -\frac{1}{512} T_5(2r-1) - \frac{1}{128} T_4(2r-1) + \right. \\ & \frac{3}{512} T_3(2r-1) + \frac{1}{32} T_2(2r-1) - \frac{1}{256} T_1(2r-1) - \\ & \left. \frac{3}{128} T_0(2r-1) \right] \left[ \frac{1}{128} T_4(2z) - \frac{7}{32} T_2(2z) + \right. \\ & \left. \frac{99}{128} T_0(2z) \right] \quad (4.57) \end{aligned}$$

in which the subscripts  $i$  and  $j$  of  $\psi_{ij}$  denote the highest degree Chebyshev function in  $r$  and  $z$ , respectively.

It may appear that the above Chebyshev series for  $\psi$  (eq. 4.57) does not follow the form given in eqn 4.28b for the Galerkin method, in that there is only one temporal coefficient,  $\psi_{54}(t)$ , for all eighteen distributed products  $T_i(r)T_j(z)$ . However, there is only one mode being considered

here, so that each constituent part of the flow moves together with the whole. The temporal coefficient is the same for each term and may be factored out.

The flow field appears as in Fig. 15 for constant unit temporal coefficients.

In the case of the temperature expansion, the choice of terms is based upon physical arguments from experimental findings. The two phenomena that are significant are the vertical redistribution of heat due to convection and the strong correlation between the temperature distribution and the vertical velocity (Shirer, 1987). The temperature function can be decomposed into a two-term expansion incorporating these features:

$$T(r, z, t) = T^1(r, z, t) + T^2(r, z, t) \quad (4.58)$$

The strong correlation between the temperature distribution and the vertical velocity  $v_z$  allows use of a temperature profile similar to that of the vertical velocity  $v_z$ . Two separate thermal boundary conditions are considered for the side wall. In the case of a conducting side wall, the temperature perturbation is zero at the wall, and the temperature distribution  $T^1(r, z, t)$  (Figs. 16, 17) is assumed to be the same as that of  $v_z$  (Figs. 11, 14):

$$T^1(r, z, t) = T^1(t) T^1(r) T^1(z) \quad (4.59a)$$

$$= T_{34}(t) [-5r^3 + 6r^2 - 1] [16z^4 - 8z^2 + 1] \quad (4.59b)$$

For the case of insulated sides, in which the derivative of the temperature with respect to  $r$  is equal to zero, a fifth degree polynomial that approximates the  $r$ -variation but with a zero  $r$ -derivative at  $r = 1$  is chosen (Figs. 18, 19):

$$T^1(r, z, t) = T^1(t) T^1(r) T^1(z) \quad (4.60a)$$

$$= T_{54}(t) [6.0r^5 - 11.3r^4 + 2.0r^3 + 4.6r^2 - 1] *$$

$$[16z^4 - 8z^2 + 1] \quad (4.60b)$$

The coefficients for this polynomial are rounded to the nearest tenth. In the attempt to construct a curve similar to the conducting case profile at every point except near the side wall, the following conditions were used:

$$\cdot T(0, z, t) = -1 \quad (\text{same } T\text{-intercept}) \quad (4.61)$$

$$\cdot T(.558, z, t) = 0 \quad (\text{same } r\text{-intercept}) \quad (4.62)$$

$$\cdot T(1, z, t) = .28 \quad (\text{same maximum } T \text{ value}) \quad (4.63)$$

$$\cdot T'(0, z, t) = 0 \quad (\text{minimum } T \text{ at } r = 0) \quad (4.64)$$

$$\cdot T'(1, z, t) = 0 \quad (r\text{-derivative of } T = 0 \text{ at } r=1) \quad (4.65)$$

$$\cdot T'(.528, z, t) = 2.02 \quad (\text{same slope at } r\text{-intercept}) \quad (4.66)$$

The relative maximum over  $r \in [0, 1]$  of the resulting curve is not at the side wall, but at  $r \approx .857$ . Its value of  $\sim .297$  does not vary sufficiently from the conducting side wall

maximum of .280 to cause undue concern. The two different distributions are compared in Fig. 20.

The second term of the temperature expansion represents the vertical redistribution of heat due to convection. Relative to the linear conductive temperature distribution, convection heats the fluid at the top of the container and cools the fluid at the bottom. This antisymmetric distribution is independent of  $r$ , and it can be represented by a cubic polynomial (Fig. 21):

$$T^2(r, z, t) = T_{03}(t) [-32z^3 + 8z] \quad (4.67a)$$

$$= T_{03}(t) [-T_3(2z) + T_1(2z)] \quad (4.67b)$$

The final Chebyshev series for the two temperature expansions are, for conducting sides,

$$\begin{aligned} T(r, z, t) = T_{34}(t) & \left[ -\frac{5}{32}T_3(2r-1) - \frac{3}{16}T_2(2r-1) + \frac{21}{32}T_1(2r-1) - \right. \\ & \left. \frac{5}{16}T(2r-1) \right] \left[ \frac{1}{8}T_4(2z) - \frac{1}{2}T_2(2z) + \frac{3}{8}T_0(2z) \right] + \\ & T_{03}(t) [-T_3(2z) + T_1(2z)] \end{aligned} \quad (4.68)$$

and for the insulated side wall,

$$\begin{aligned} T(r, z, t) = T_{54}(t) & [6.0r^5 - 11.3r^4 + 2.0r^3 + 4.6r^2 - 10] * \\ & [16z^4 - 8z^2 + 1] + T_{03}(t) [-32z^3 + 8z] \end{aligned} \quad (4.69a)$$

$$\begin{aligned}
&= T_{54}(t) \left[ \frac{6}{512} T_5(2r-1) + \frac{37}{1280} T_4(2r-1) - \right. \\
&\quad \frac{3725}{32000} T_3(2r-1) - \frac{925}{8000} T_2(2r-1) + \frac{483}{640} T_1(2r-1) - \\
&\quad \left. \frac{11857}{1280} T_0(2r-1) \right] \left[ \frac{1}{8} T_4(2z) - \frac{1}{2} T_2(2z) + \frac{3}{8} T_0(2z) \right] + \\
&T_{03}(t) [-T_3(2z) + T_1(2z)] \tag{4.69b}
\end{aligned}$$

#### 4.4 Chebyshev-Galerkin Spectral Method

The Galerkin spectral method converts the perturbed Boussinesq system into a system of ordinary differential equations in the temporal coefficients. The reason for this transformation is that stability theory for systems of ordinary differential equations is much easier and more refined than for systems of partial differential equations. Although this system models the flow in the conductive and laminar flow regimes, it is the mathematical stability of the system and the physical stability of the modeled flow itself that are actually being considered.

The inaccuracy inherent in the representation of the dependent variables  $\psi$  and  $T$  by approximate Chebyshev series is mitigated by the weighted residual technique of this method.

The general procedure (e.g., Canuto et al., 1990) is as follows.

Let the perturbed Boussinesq system be represented by

$$\frac{\partial \mathbf{u}}{\partial t} - M(\mathbf{u}) = 0 \quad (4.70)$$

in which

$$\mathbf{u}(r, z, t) = (\psi(r, z, t), T(r, z, t)) \quad (4.71)$$

The Chebyshev series approximation for  $\mathbf{u}$  is

$$\mathbf{u}^N(r, z, t) = \sum_{k=1}^N \mathbf{a}_k(t) \mathbf{u}_k(r) \mathbf{u}_k(z) \quad (4.72a)$$

$$= \sum_{k=1}^N \mathbf{a}_k(t) \left[ \sum_{i=0}^P b_i T_i(r) \right] \left[ \sum_{j=0}^R c_j T_j(z) \right] \quad (4.72b)$$

These expansions may not satisfy eq. 4.70 exactly over the whole interval, the residuals

$$\frac{\partial \mathbf{u}^N}{\partial t} - M(\mathbf{u}^N) \quad (4.73)$$

not being everywhere zero. The optimal solution is obtained by requiring that the integrals of the weighted residuals,

$$\int_{-\frac{1}{2}}^{\frac{1}{2}} \int_0^1 \left[ \frac{\partial \mathbf{u}^N}{\partial t} - M(\mathbf{u}^N) \right] \phi_k(r) \phi_k(z) dr dz = 0, \quad k = 1, \dots, N \quad (4.74)$$

vanish over the interval.

The residual is weighted by the test functions  $\phi(r)$  and  $\phi(z)$ . These two functions are chosen to be orthogonal to the corresponding spatial expansions  $u_k$  over the interval:

$$\int_0^1 u_k(r) \phi_1(r) dr = c_1 \delta_{k1}, \quad c_1 \in \mathbb{R}, c_1 \neq 0 \quad (4.75)$$

$$\int_{-\frac{1}{2}}^{\frac{1}{2}} u_k(z) \phi_1(z) dz = c_2 \delta_{k1}, \quad c_2 \in \mathbb{R}, c_2 \neq 0 \quad (4.76)$$

in which  $\delta_{kl}$  is the Kronecker delta.

In the Galerkin method, test functions are chosen to be the same type of functions as in the spatial expansions, in this case, Chebyshev functions. For a single Chebyshev function  $T_i(x)$ , the test function is

$$\frac{T_j(x)}{\sqrt{1-x^2}} \quad (4.77)$$

The weighted orthogonality condition is:

$$\int_{-1}^1 T_i(x) \frac{T_j(x)}{\sqrt{1-x^2}} dx = \begin{cases} 0 & i \neq j \\ \frac{\pi}{2} & i=j \neq 0 \\ \pi & i=j=0 \end{cases} \quad (4.78)$$

The weight is the radical denominator. For a spatial expansion consisting of a finite Chebyshev series, such as

$$u(x) = \sum_{i=0}^P b_i T_i(x) \quad (4.79)$$

one possible test function is:

$$\phi(x) = \frac{\sum_{i=0}^P b_i T_i(x)}{\sqrt{1-x^2}} \quad (4.80)$$

The result of the orthogonality in this case is

$$\int_{-1}^1 u(x) \phi(x) dx = \int_{-1}^1 \left[ \sum_{i=0}^P b_i T_i(x) \right] \left[ \frac{\sum_{i=0}^P b_i T_i(x)}{\sqrt{1-x^2}} \right] dx \quad (4.81a)$$

$$= \pi \left[ b_0^2 + \frac{1}{2} (b_1^2 + b_1^2 + \dots + b_P^2) \right] \quad (4.81b)$$

This particular test function is chosen for two reasons. The first is that having the sum of the squares of the Chebyshev coefficients  $b_i$  (eq. 4.81b) ensures that the entire set of temporal coefficients  $a_k(t)$  of equation 4.72 will always appear in the equation, never taking a value of zero. The second reason is that each constituent part is certain to be represented. This type of test function is applied consistently to all three derived equations.

Once these test functions have been determined, the system of integral equations can be solved, resulting in a low-order system of ordinary equations in the temporal coefficients:

$$\frac{da_k}{dt} - f(a_k) = 0 \quad k = 1, 2, \dots, N \quad (4.82)$$

This Chebyshev-Galerkin spectral method is applied first to the case of conducting side walls. This situation is algebraically easier than the insulated side wall case because of the less complex form of the temperature expansion. The  $T_{34}(t)$  equation is found first to illustrate the method.

The  $T_{34}(t)$  equation is derived from the perturbed energy equation, which contains the time derivative of  $T$  and therefore the time derivative of its component  $T_{34}(t)$ .

The expansions for the stream function  $\psi$  and the temperature for conducting side walls,

$$\psi(r, z, t) = \psi_{54}(t) \psi(r) \psi(z) \quad (4.83a)$$

$$\begin{aligned} &= \psi_{54}(t) \left[ -\frac{1}{512} T_5(2r-1) - \frac{1}{128} T_4(2r-1) + \right. \\ &\quad \left. \frac{3}{512} T_3(2r-1) + \frac{1}{32} T_2(2r-1) - \frac{1}{256} T_1(2r-1) - \right. \\ &\quad \left. \frac{3}{128} T_0(2r-1) \right] \left[ \frac{1}{128} T_4(2z) - \frac{7}{32} T_2(2z) + \right. \\ &\quad \left. \frac{99}{128} T_0(2z) \right] \end{aligned} \quad (4.83b)$$

and

$$T(r, z, t) = T_{34}(t) T^1(r) T^1(z) + T_{03}(t) T^2(z) \quad (4.84a)$$

$$= T_{34}(t) \left[ -\frac{5}{32} T_3(2r-1) - \frac{3}{16} T_2(2r-1) + \frac{21}{32} T_1(2r-1) - \right.$$

$$\left. \frac{5}{16} T(2r-1) \right] \left[ \frac{1}{8} T_4(2z) - \frac{1}{2} T_2(2z) + \frac{3}{8} T_0(2z) \right] +$$

$$T_{03}(t) [-T_3(2z) + T_1(2z)] \quad (4.84b)$$

are substituted into the perturbed energy equation,

$$\frac{\partial T}{\partial t} + \frac{1}{r} J(\psi, T) - \frac{1}{r} \frac{\partial \psi}{\partial r} - \nabla^2 T = 0 \quad (4.85)$$

The equation is then multiplied by the test functions for  $T_{34}(t)$  and integrated over the domain:

$$\int_{-\frac{1}{2}}^{\frac{1}{2}} \int_0^1 \left\{ \frac{\partial T}{\partial t} + \frac{1}{r} J(\psi, T) - \frac{1}{r} \frac{\partial \psi}{\partial r} - \nabla^2 T \right\} \phi(r) \phi(z) dr dz = 0 \quad (4.86)$$

where the test functions for  $T_{34}(t)$  are

$$\phi(r) = \frac{2T_1(r)}{\sqrt{1-(2r-1)^2}} a) \quad (4.87a)$$

$$= \frac{2 \left[ -\frac{5}{32} T_3(2r-1) - \frac{3}{16} T_2(2r-1) + \frac{21}{32} T_1(2r-1) - \frac{5}{16} T(2r-1) \right]}{\sqrt{1-(2r-1)^2}}$$

$$(4.87b)$$

and

$$\phi(z) = \frac{2T_1(z)}{\sqrt{1-(2z)^2}} \quad (4.88a)$$

$$= \frac{2\left[\frac{1}{8}T_4(2z) - \frac{1}{2}T_2(2z) + \frac{3}{8}T_0(2z)\right]}{\sqrt{1-(2z)^2}} \quad (4.88b)$$

The coefficient "2" in the numerator of the test functions is the constant resulting from the transformation of eq. 4.78 in  $x$  to one in either  $2r-1$  or  $2z$ .

The software package "Mathematica" was used to perform the integration. The capabilities of this software are such that each term must be evaluated separately. The resulting equation for the time variation in  $T_{34}(t)$  is:

$$T'_{34}(t) = \psi_{54}(t) - \frac{138728}{4095}T_{34}(t) - \frac{28}{5}\psi_{54}(t)T_{03}(t) \quad (4.89)$$

Note that the equation is nonlinear, and that all terms have been retained from the original equation.

This procedure is repeated to obtain the  $T_{03}(t)$  equation from the energy equation and the  $\psi(t)$  equation from the Navier-Stokes equations to complete the system:

$$T'_{03}(t) = -T_{03}(t) + \frac{777}{2048}\psi_{54}(t)T_{03}(t) \quad (4.90)$$

$$\psi'_{54}(t) = -\frac{17868}{355}\text{Pr}\psi_{54}(t) + \frac{42}{71}\text{PrRa}T_{34}(t) \quad (4.91)$$

In the  $T'_{03}(t)$  equation, note that the integration of the

$(-1/r)(\partial\psi/\partial r)$  term produces a zero. In the  $\psi'(t)$  equation, the term derived from the  $\mathbf{v} \cdot \nabla \mathbf{v}$  term of the perturbed Boussinesq system is zero. The absence of this nonlinear term in the case of a low-Prandtl number fluid would be significant if the stability of any convective flow regime with its finite velocity vectors were being considered. In the present work, however, conductive stability with its zero velocity vector is of interest, and the loss of this inertial term has no effect.

These same features can be seen in the case of insulated side walls. The same Chebyshev-Galerkin procedure is followed, the difference being the use of the insulated form of the temperature expansion and its test function.

$$\psi'_{54}(t) = -\frac{17868}{355} \text{Pr} \psi_{54}(t) + \frac{2765}{426} \text{Pr Ra } T_{54}(t) \quad (4.92)$$

$$T'_{54}(t) = \frac{114636}{1205993} \psi_{54}(t) - \frac{38915152}{1361605} T_{54}(t) - \frac{3209800}{6029965} \psi_{54}(t) T_{03}(t) \quad (4.93)$$

$$T'_{03}(t) = -48 T_{03}(t) + \frac{63805}{16384} \psi_{54}(t) T_{54}(t) \quad (4.94)$$

In form, this system is similar to that of the conducting side wall case, the only difference being the replacement of the  $T_{03}(t)$  term in the nonlinear term in the  $T'_{03}(t)$  equation (4.90) with  $T_{54}(t)$ . The most noticeable difference is that the magnitudes of the coefficients of  $T_{54}(t)$  are relatively

larger in this insulated set of equations than those of the coefficients of  $T_{34}(t)$  in the conducting case. This increase may introduce more damping of the growth of the stream function variable and consequently of the flow.

Both of these systems of first order ordinary differential equations are now in a form amenable to stability analysis. The small number of equations is a reflection of the relative simplicity of the laminar axisymmetric flow. In the stability analysis of the next chapter, the critical point of transition from the conductive regime to the convective regime is determined.

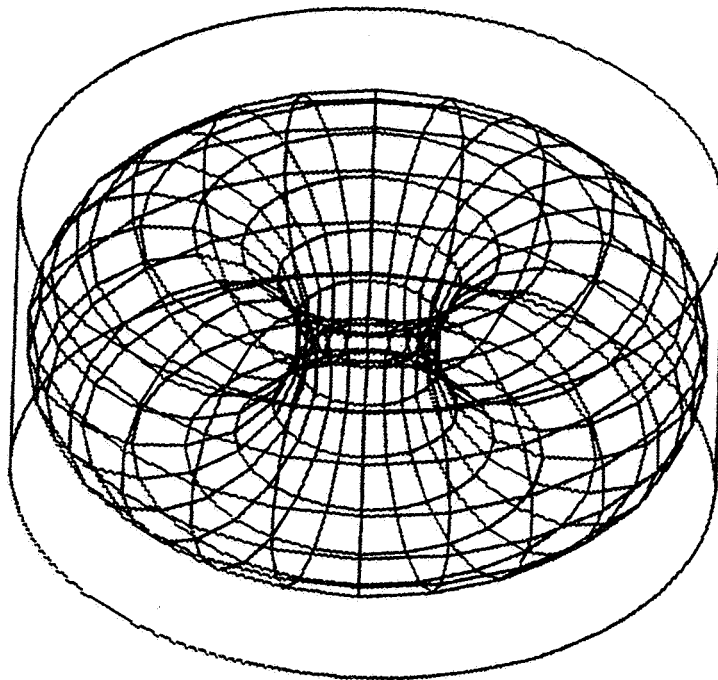


**Figure 9.** Toroidal shape of axisymmetric convection cell.

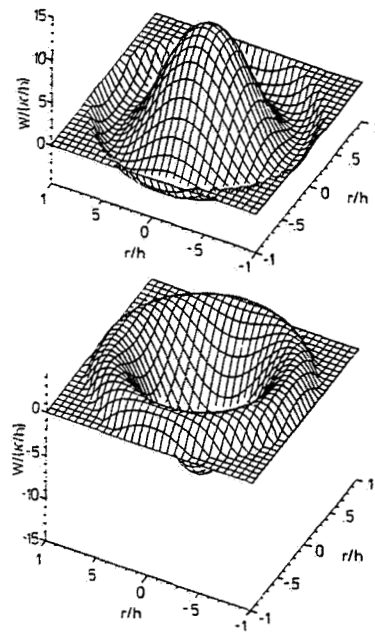


**Figure 10.** Laminar axisymmetric flow field,  $\gamma=1$ , for water ( $\text{Pr}=6.7$ ) (Müller et al., 1984).

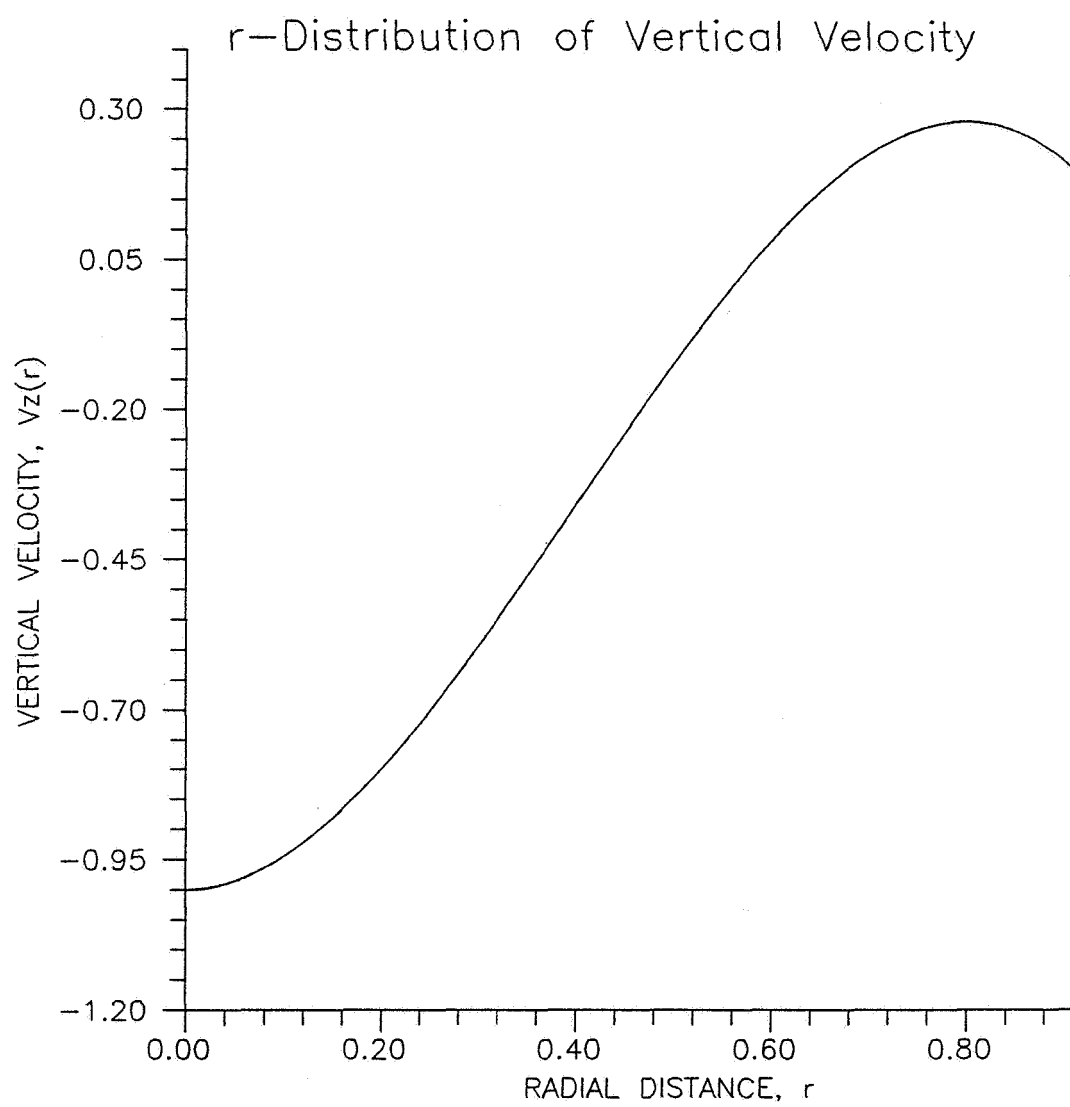


**Figure 11.** r-variation of  $v_z$ .

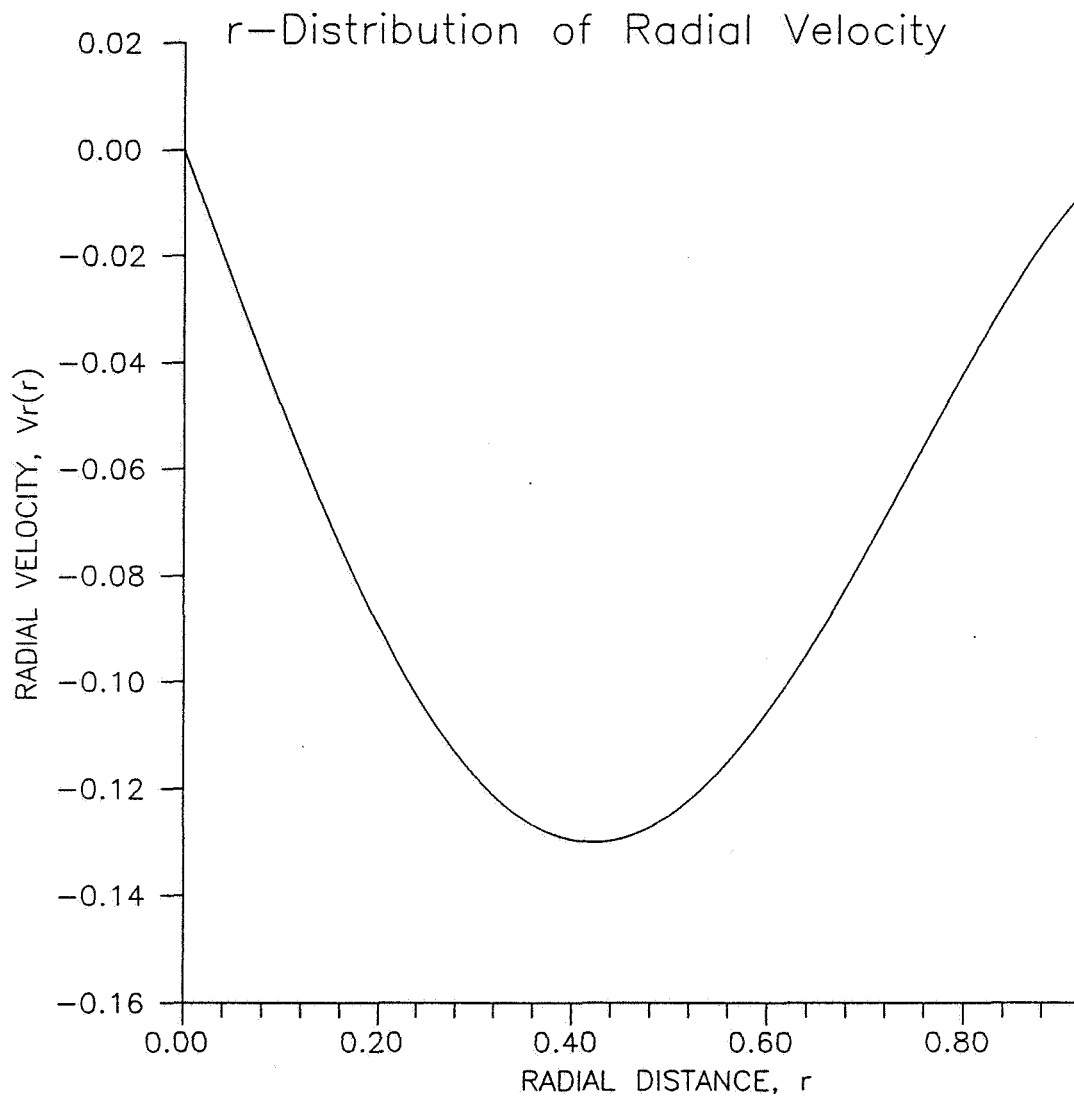


**Figure 12.**  $r$ -variation of  $v_r$ .

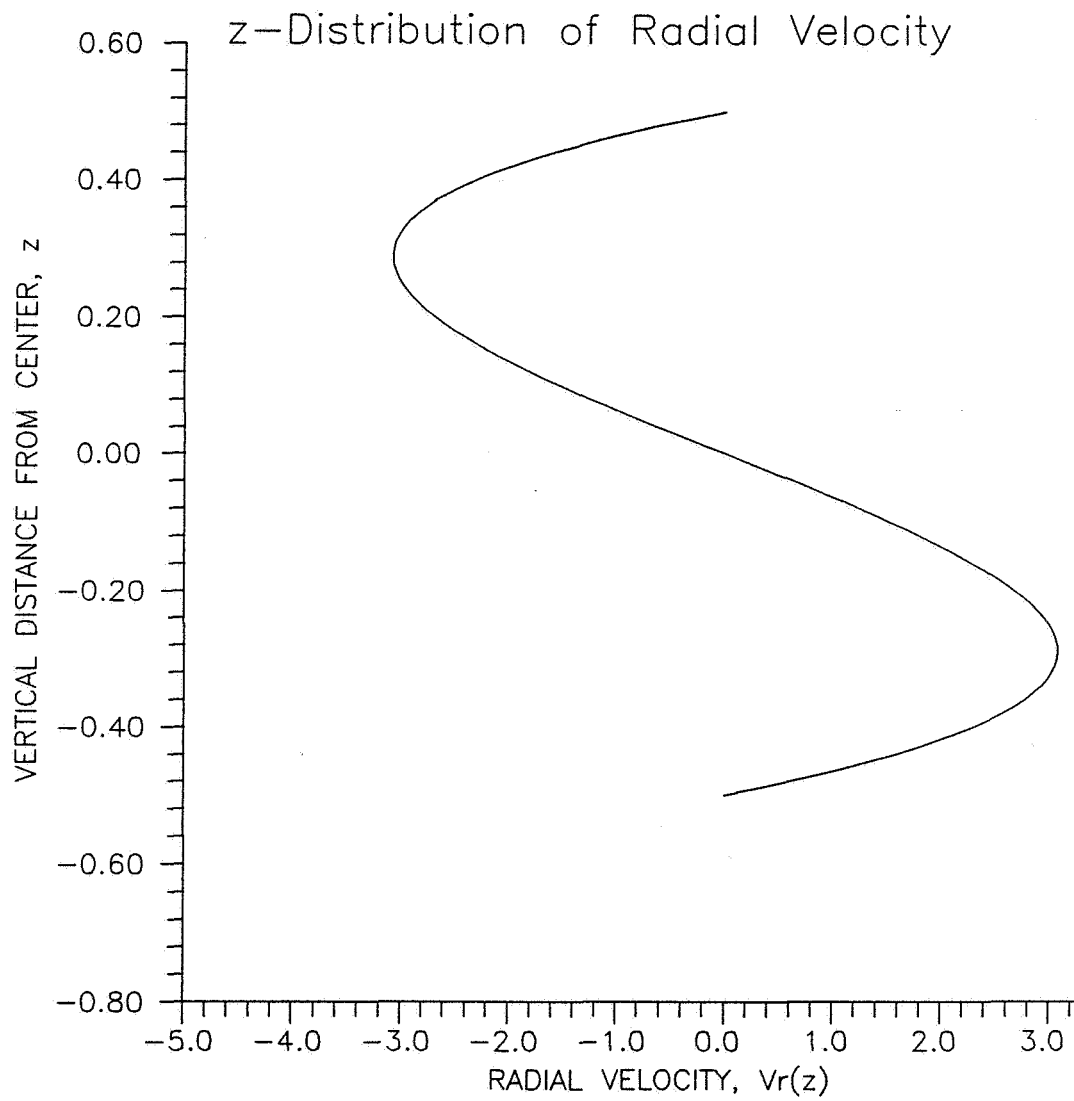


**Figure 13.**  $z$ -variation of  $v_r$ .

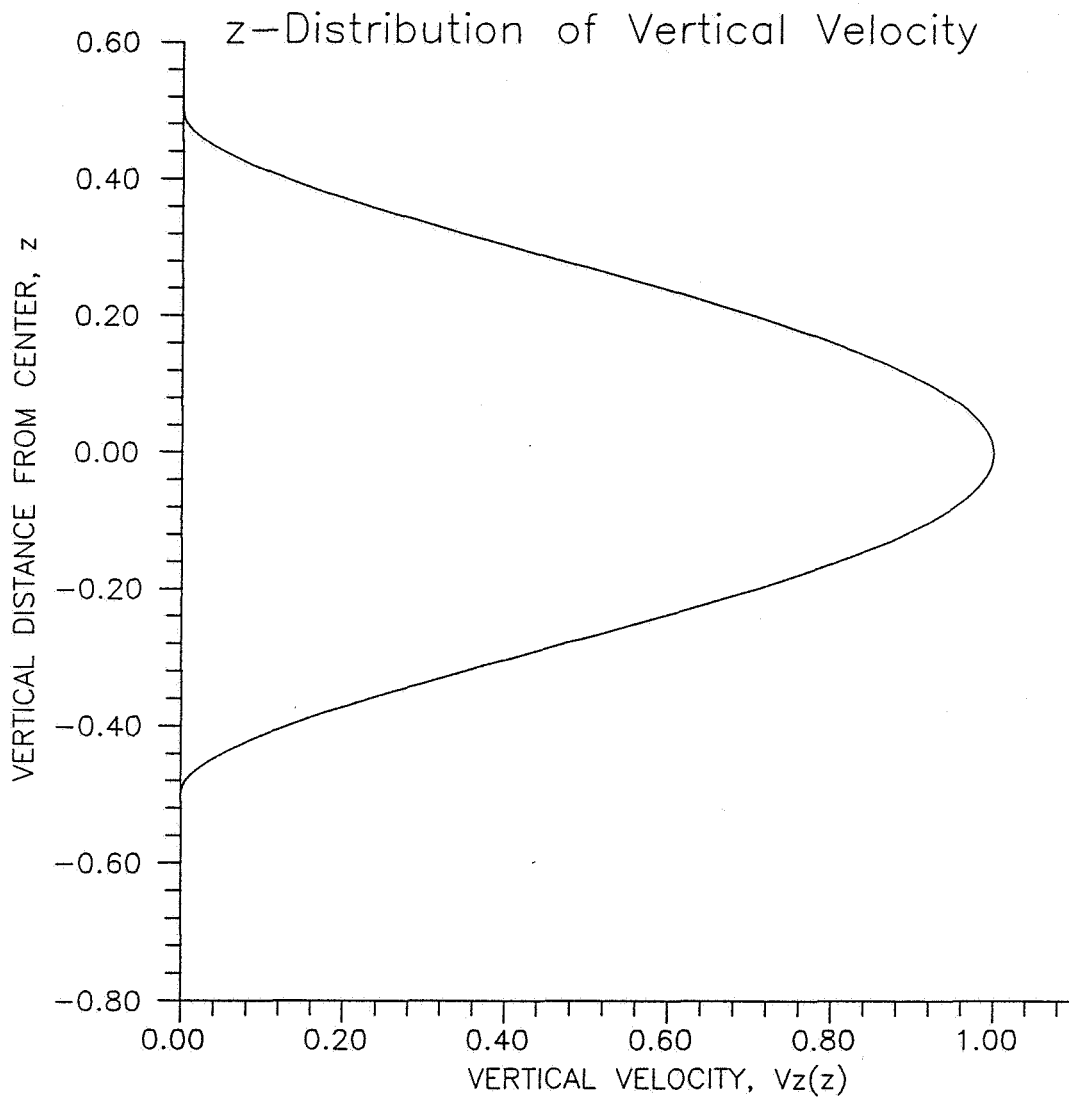


**Figure 14.**  $z$ -variation of  $v_z$ .

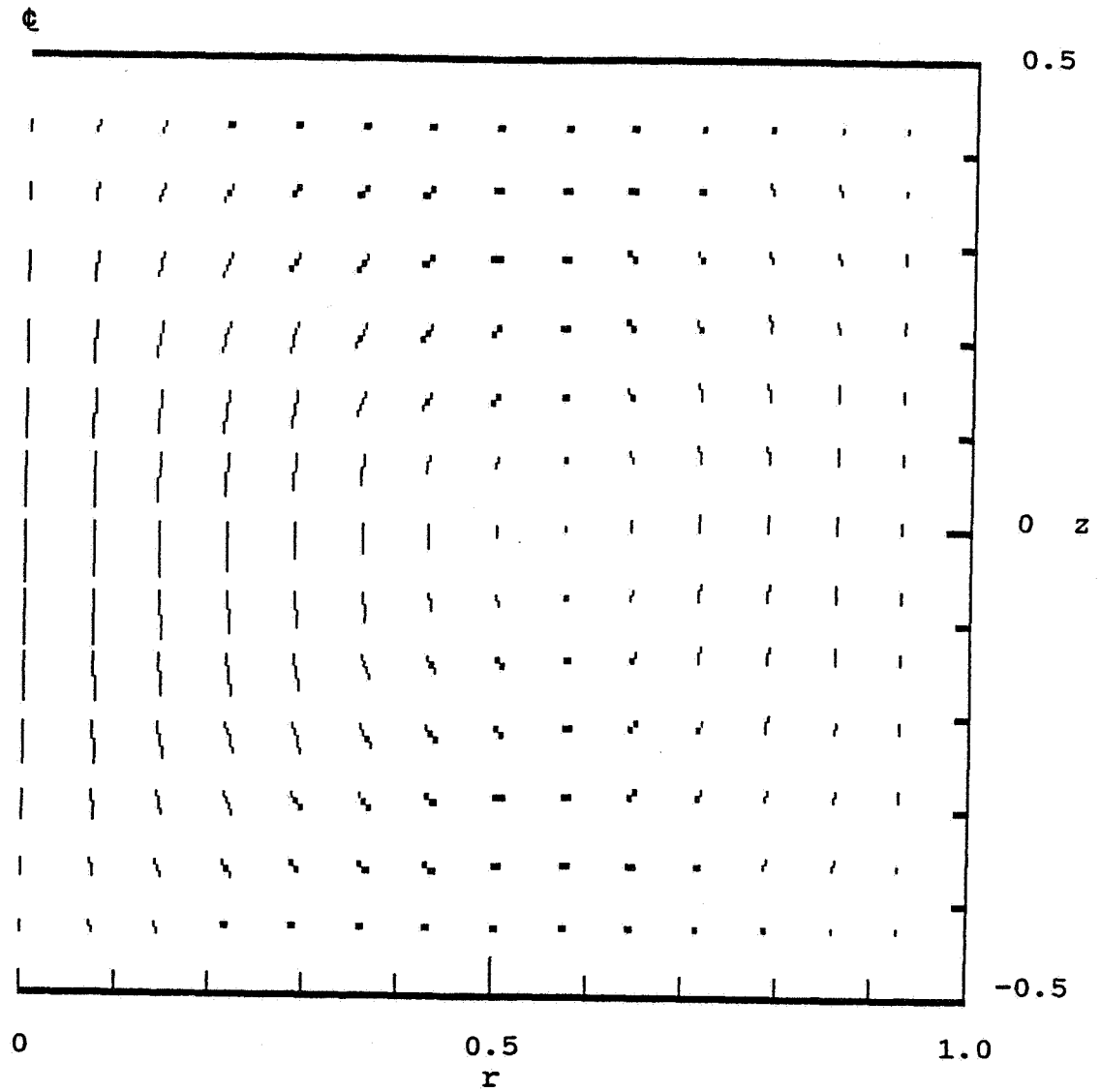


**Figure 15.** Axisymmetric flow field for  $\psi(r,z)$  in half-section of cylinder with  $\gamma=1$ . Flow rotates counterclockwise, falling at the center.

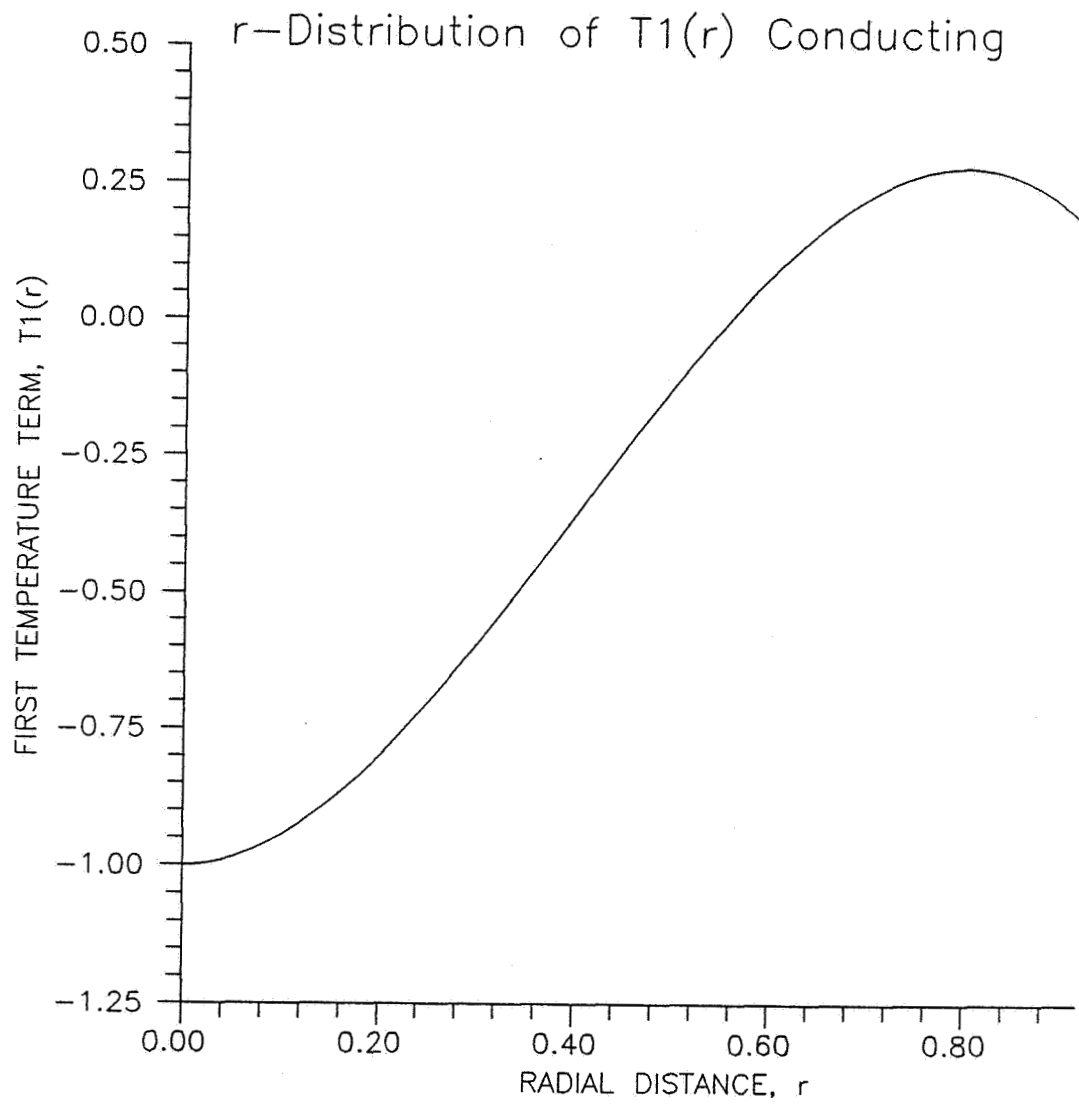


**Figure 16.** r-variation of conducting  $T^1(r,z,t)$  expression.

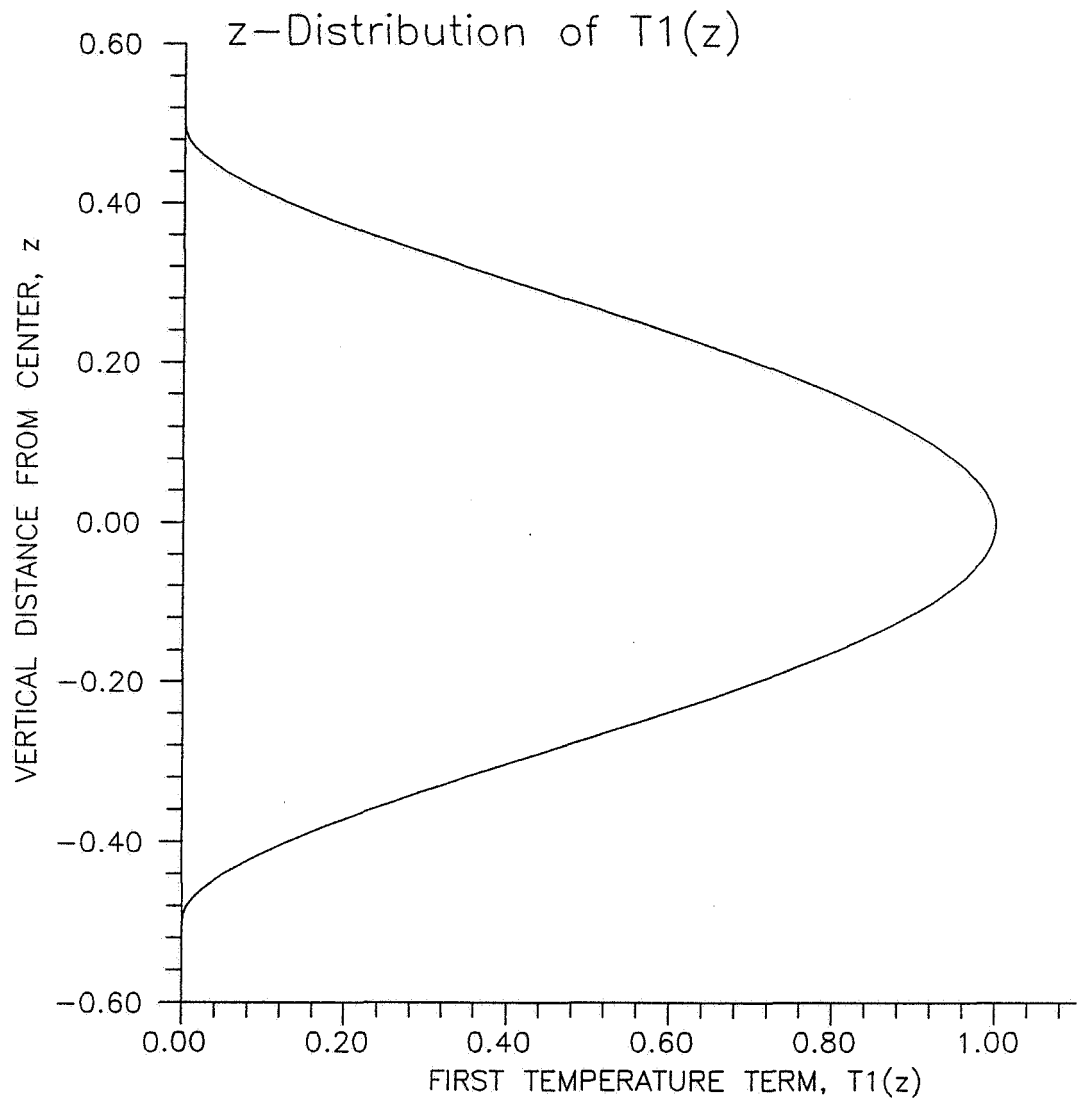


**Figure 17.**  $z$ -variation of conducting  $T^1(r, z, t)$  expression.

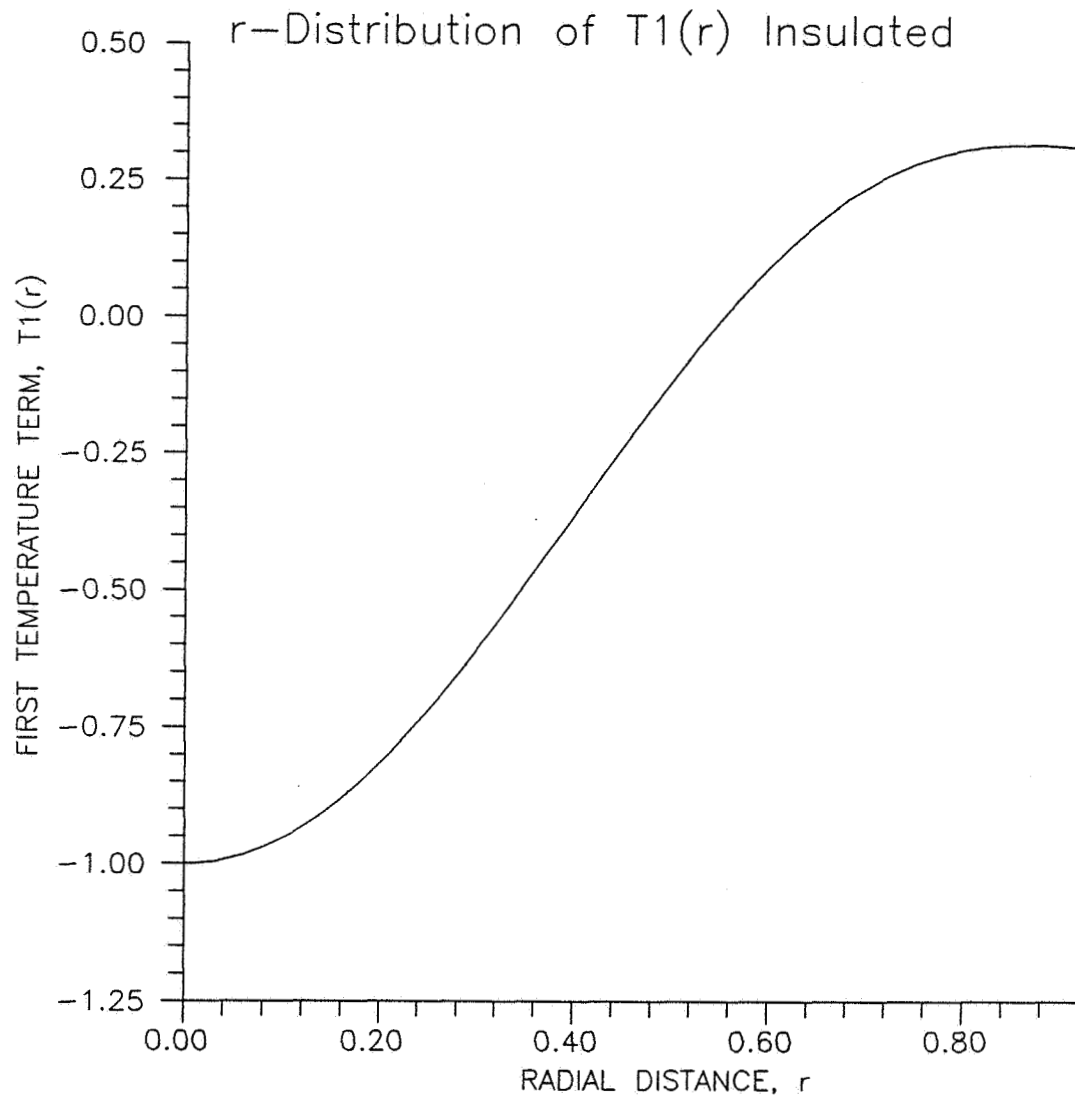


**Figure 18.**  $r$ -variation of insulated  $T^1(r,z,t)$  expression.

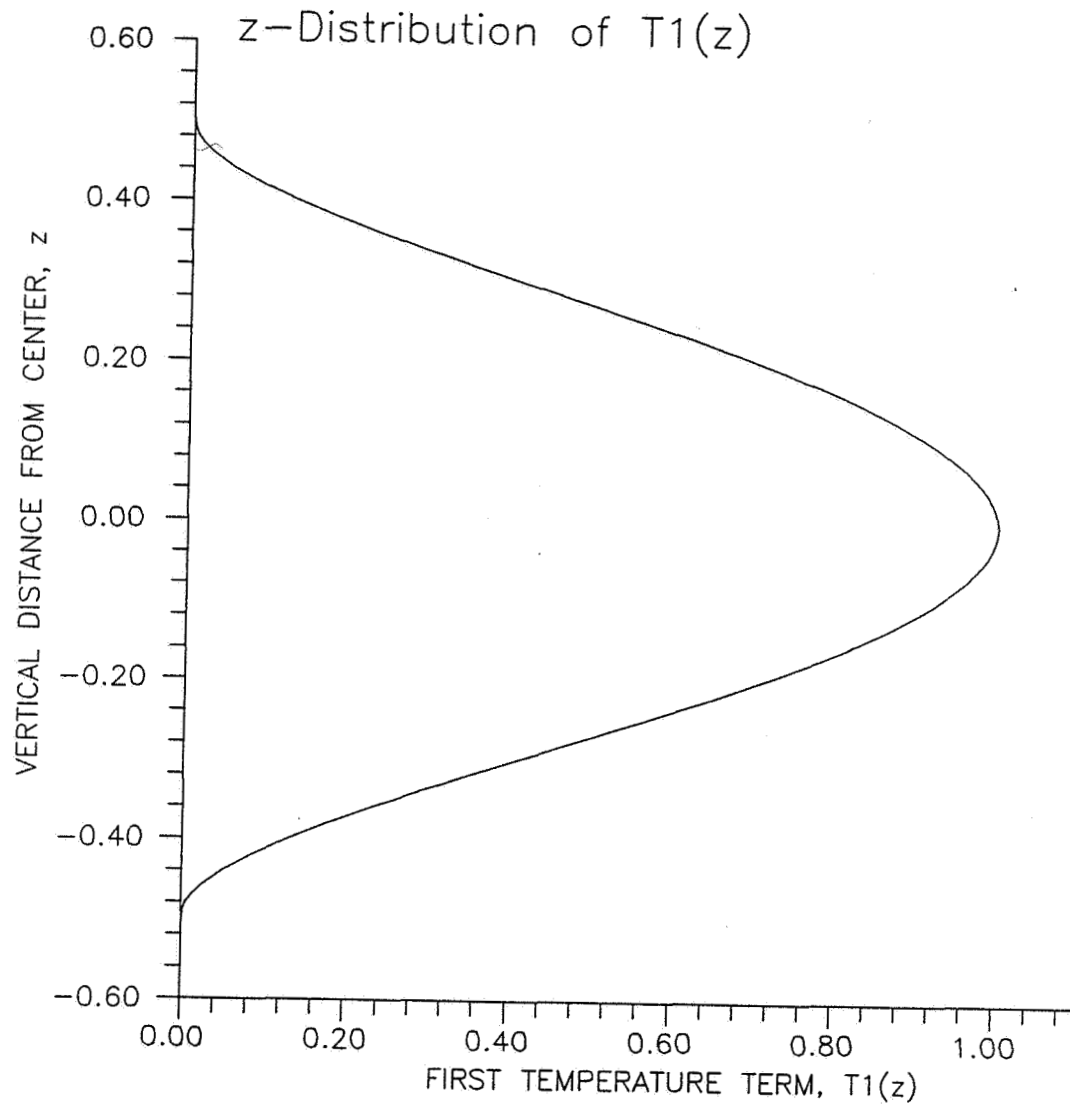


**Figure 19.**  $z$ -variation of insulated  $T^1(r,z,t)$  expression.

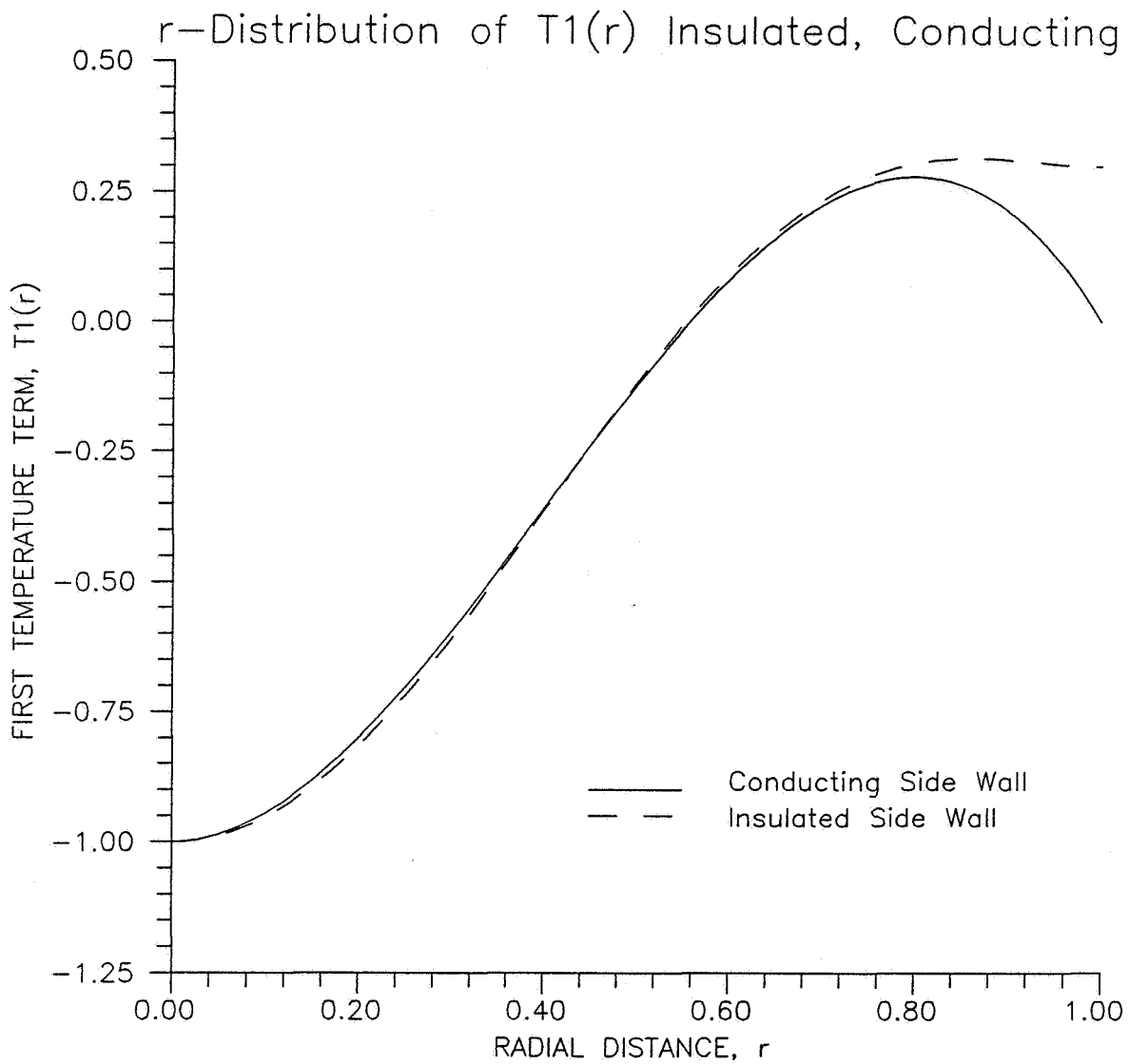


**Figure 20.**  $r$ -variations of insulated, conducting  $T^1(r,z,t)$  expressions.

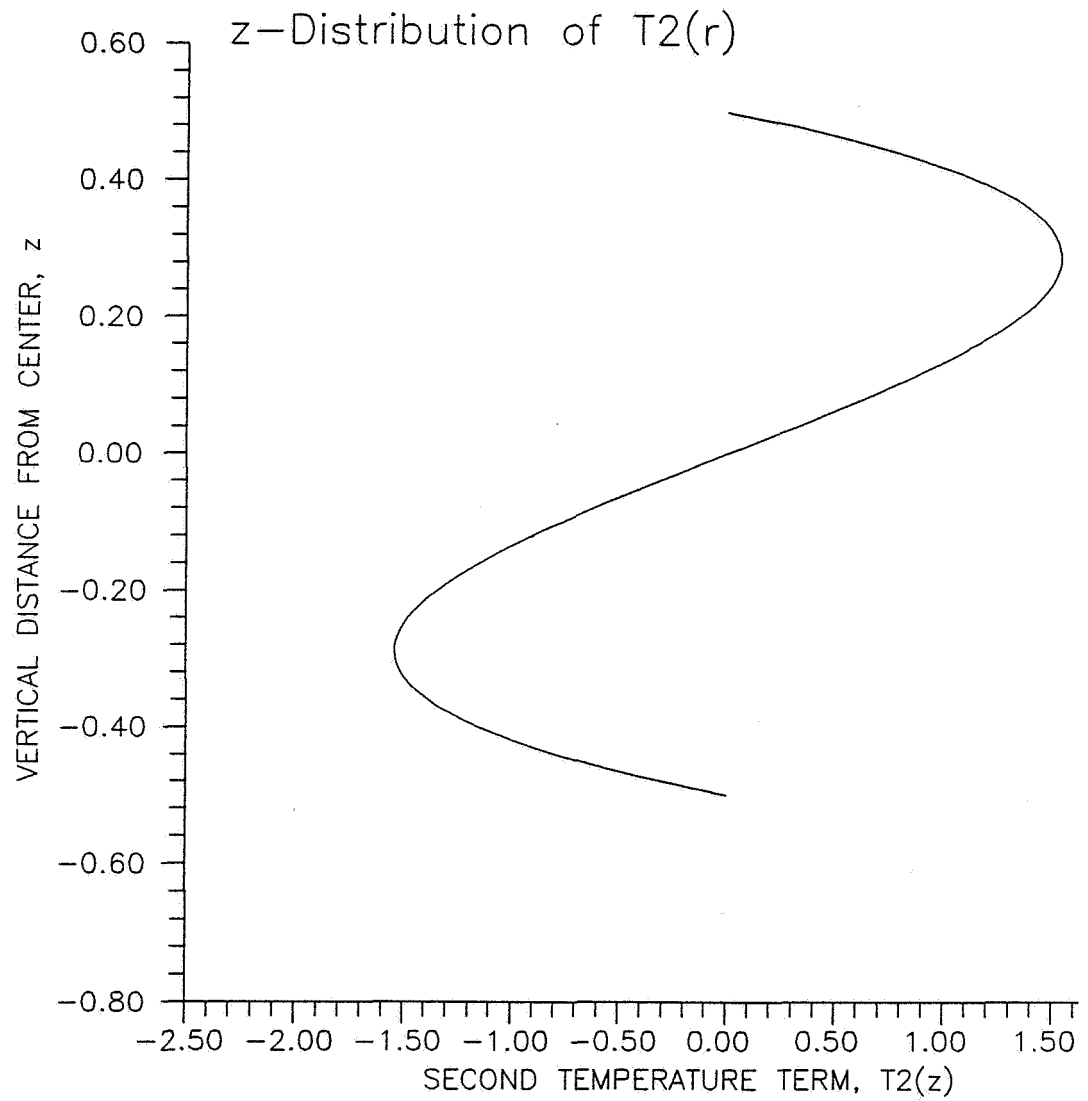


**Figure 21.**  $z$ -variation of  $T^2(r, z, t)$  expression.

## CHAPTER 5. LOCAL STABILITY ANALYSIS

The crystal melt exhibits a number of different flow patterns on the route to turbulence, from the conductive state of quiescent flow, through laminar and periodic convective flows, to full-scale turbulent convection (e.g., Knuteson, 1989). The point of transition at which the onset of a new flow regime occurs is called a bifurcation. The Rayleigh number values at these points of bifurcation are known as critical Rayleigh numbers, and they are numbered in the order in which they occur. In this study, the critical Rayleigh number at the onset of laminar convection, the first critical Rayleigh number,  $Ra_{c1}$ , is determined.

Each of the different flow regimes is "stable" over its particular range of the Rayleigh number. A stable flow regime is one in which the physical perturbations induced by changes in the forcing temperature gradient are sufficiently damped by viscosity and thermal conductivity to maintain the distinct qualitative characteristics of the flow. Flow instability at the bifurcation is caused by the undamped growth of perturbations, resulting in time in a qualitatively different flow pattern (e.g., Gelaro, 1987). To determine the stability of a flow or the stability of its mathematical model is to determine the bifurcations.

The flow patterns in the melt are characterized by

greater complexity and loss of regularity as the Rayleigh number is increased. The stability of the corresponding solutions of the mathematical model can themselves be categorized by their degree of complexity. Bifurcations are either local or global, depending upon the degree of regularity of the temporal behavior of the solution (e.g., Thompson and Stewart., 1986). For the two systems of ordinary differential equations derived in the last chapter, the local bifurcation at the transition from conduction to laminar convection will be examined. The stability analysis is then said to be a local stability analysis.

The local stability analysis of systems of ordinary differential equations that are nonlinear is difficult to approach directly. If possible, the system is simplified by a reduction of dimension or by a linearization technique (e.g., Wiggins, 1990). The linearization approach is pursued in the present study. The determinant of coefficients of the linearized system is examined to determine the first critical Rayleigh number (e.g., Gelaro, 1987) for both the conducting and insulated side wall cases.

### **5.1 Local Bifurcation Theory**

Local bifurcations are those changes in stability that

occur for relatively simple flow patterns and solutions (e.g., Argyris et al., 1991). For Rayleigh-Bénard convection, the initial conductive state and the laminar and periodic convective flow patterns are either steady or repetitive in nature. The solutions of the systems of equations derived in the last chapter reflect this simplicity. Procedures for determining the stability of these solutions are fairly straightforward (e.g., Wiggins, 1990). On the other hand, flow regimes past the periodic are more complex spatially and temporally. Determination of these global bifurcations is therefore more difficult (e.g., Wiggins, 1990).

In the present study, for example, consider the solution vector  $(\psi_{54}(t), T_{54}(t), T_{03}(t))$  for the case of the insulated side wall. For the conductive solution, all convective perturbations are zero, so that the solution is the zero vector  $(\psi_{54}(t), T_{54}(t), T_{03}(t)) = (0, 0, 0)$ . This is a single point in the solution plot, it is time-invariant, and it is decidedly "local" in nature. Similarly, for fixed Rayleigh number, the plot of the time-invariant solution for laminar convection consists of two distinct points (e.g., Thompson and Stewart., 1986). A solution need not be time-invariant to be local. The periodic solution is also local because its three-dimensional solution plot or "trajectory" is fixed in the solution space and does not vary beyond one period. The solutions are "local" in the sense that their trajectories

have a decidedly simple structure in the solution plot. The plots of "global" solutions, on the other hand, have a more complex structure and occupy a larger portion of the solution space (e.g., Argyris, 1991). The loss of stability--the bifurcation--is the transition from one solution or structure to another. It is the stability of the conductive solution and structure in the vicinity of the first critical Rayleigh number that is of interest in the present study. To investigate the stability of the conductive regime of the liquid melt, the stable conductive solution must first be found. It is the time-invariance of this "stationary" solution that allows it to be determined easily.

## 5.2 Stationary Solutions

Stationary solutions are the time-invariant solutions of a system of ordinary differential equations. In the present study they are necessary for the local stability analysis because they are the base state in the perturbation procedure of the linear approximation. The definition and general procedure for their determination are as follows (e.g., Wiggins, 1990). Consider a system of ordinary differential equations

$$\frac{d\mathbf{x}}{dt} = f(\mathbf{x}), \quad \mathbf{x} \in \mathbb{R}^n, n \in \{1, 2, 3, \dots\} \quad (5.1)$$

"Stationary" solutions are those solutions

$$\bar{\mathbf{x}} \in \mathbb{R}^n \quad (5.2)$$

such that

$$f(\bar{\mathbf{x}}) = 0 \quad (5.3)$$

Stationary solutions are solutions that do not change over time. Each system is characterized by a set of time-invariant or "stationary" convective solutions representing the conductive and laminar convective flow regimes. This definition does not imply that the flow itself is physically stationary, but that the flow pattern is stable and does not vary over its own temporal scale. For example, laminar flow is stationary but is certainly not quiescent. The stationary flows represented by such stationary solutions often exhibit variance in the flow near flow transitions if sufficiently perturbed, but these flows are transient (e.g., Thompson and Stewart., 1986).

In the present study, the system is expressed in terms of the temporal convective perturbations of the flow,  $\psi_{54}(t)$ , and of the temperature,  $T_{34}(t)$  or  $T_{54}(t)$ , and  $T_{03}(t)$ . The stationary solutions of the nonlinear system for the conducting side wall,

$$\psi'_{54}(t) = -\frac{17868}{355} \text{Pr} \psi_{54}(t) + \frac{42}{71} \text{PrRa} T_{34}(t) \quad (5.4)$$

$$T'_{34}(t) = \psi_{54}(t) - \frac{138728}{4095} T_{34}(t) - \frac{28}{5} \psi_{54}(t) T_{03}(t) \quad (5.5)$$

$$T'_{03}(t) = -T_{03}(t) + \frac{777}{2048} \psi_{54}(t) T_{03}(t) \quad (5.6)$$

may be found by letting the time derivatives be zero,

$$\psi'_{54}(t) = T'_{34}(t) = T'_{03}(t) = 0 \quad (5.7)$$

letting the stream function and temperature variables be constant,

$$\psi_{54}(t) = \psi_{54}^S, \quad T_{34}(t) = T_{34}^S, \quad \text{and} \quad T_{03}(t) = T_{03}^S \quad (5.8)$$

and solving for these stationary variables. The three solutions that result are the conductive solution,

$$\psi_{54}^S = 0, \quad T_{34}^S = 0, \quad T_{03}^S = 0 \quad (5.9)$$

and two convective solutions,

$$\psi_{54}^S = \frac{\sqrt{-1692188606464 + 587059200\text{Ra}}}{3\sqrt{245659687}} \quad (5.10)$$

$$T_{34}^S = \frac{2\sqrt{\left(\frac{1489}{8084167}\right)(-1692188606464 + 587059200\text{Ra})}}{15\text{Ra}} \quad (5.11)$$

$$T_{03}^S = \frac{-1692188606464 + 587059200\text{Ra}}{3287531520\text{Ra}} \quad (5.12)$$

and

$$\psi_{54}^s = \frac{-\sqrt{-1692188606464 + 587059200Ra}}{3\sqrt{245659687}} \quad (5.13)$$

$$T_{34}^s = \frac{-2\sqrt{\left(\frac{1489}{8084167}\right)(-1692188606464 + 587059200Ra)}}{15Ra} \quad (5.14)$$

$$T_{03}^s = \frac{-1692188606464 + 587059200Ra}{3287531520Ra} \quad (5.15)$$

Note that these solutions are solutions of the nonlinear system. The stationary conductive solution is essentially a zero-convection stationary solution. The two convective solutions differ only in the change in sign of the  $\psi_{54}^s$  and  $T_{34}^s$  solutions. These solutions are the two different rotational directions the flow may follow--flow rising or falling in the center of the cylinder. It should be noted that the radicals in these convective solutions are imaginary for a value of the Rayleigh number less than ~2882.5. Imaginary values for the stream function and temperature variables indicate flows that do not exist. It will be shown later that this Rayleigh number is the critical Rayleigh number marking the transition between conductive and laminar convective flow. It may also be noted that the Prandtl number is not a parameter in these radicands, suggesting the possible Prandtl number-independence of this flow regime transition.

For the insulated side wall case, the solutions are the conductive state,

$$\psi_{54}^{S,I} = 0, T_{34}^{S,I} = 0, T_{03}^{S,I} = 0 \quad (5.16)$$

and the two convective solutions,

$$\psi_{54}^{S,I} = \frac{64 \sqrt{\left(\frac{2998}{146286635}\right) (-21555414014016 + 9244915750 \text{ Ra})}}{52115} \quad (5.17)$$

$$T_{34}^{S,I} = \frac{4608 \sqrt{\left(\frac{2998}{146286635}\right) (-21555414014016 + 9244915750 \text{ Ra})}}{483875 \text{ Ra}} \quad (5.18)$$

$$T_{03}^{S,I} = \frac{8198031 (-21555414014016 + 9244915750 \text{ Ra})}{421592157461282500 \text{ Ra}} \quad (5.19)$$

and

$$\psi_{54}^{S,I} = \frac{-64 \sqrt{\left(\frac{2998}{146286635}\right) (-21555414014016 + 9244915750 \text{ Ra})}}{52115} \quad (5.20)$$

$$T_{34}^{S,I} = \frac{-4608 \sqrt{\left(\frac{2998}{146286635}\right) (-21555414014016 + 9244915750 \text{ Ra})}}{483875 \text{ Ra}} \quad (5.21)$$

$$T_{03}^{S,I} = \frac{8198031 (-21555414014016 + 9244915750 \text{ Ra})}{421592157461282500 \text{ Ra}} \quad (5.22)$$

In this case, the radicals in these convective solutions are imaginary for a value of the Rayleigh number less than ~2331.6.

In the following linear approximation of the local stability analysis, the linearized system of equations is perturbed about these stationary solutions and the first

critical Rayleigh number is determined.

### **5.3 The Linear Approximation**

The two systems of ordinary differential equations that were derived in the last chapter from the perturbed Boussinesq system are strongly nonlinear. The local stability analysis of nonlinear systems of ordinary differential equations such as these is difficult to approach directly. In the present study, the system is simplified by a linearization technique (e.g., Wiggins, 1990).

The linear approximation of the nonlinear local stability of the conductive solution is approached by a perturbation method. In this second perturbation of the original Boussinesq system, the basic state is the stationary conductive solution. The system is transformed into a system in terms of the convective perturbations. By using this time-invariant basic state, the temporal decay or growth of the perturbations alone indicates respectively the persistence of conduction or the initiation of laminar convection.

In the linearized system of ordinary differential equations representing the flow, solutions are exponential expressions of the form

$$ce^{\lambda t}, \quad c \in \mathbb{R}, \lambda \in \mathbb{C} \quad (5.23)$$

in which  $\lambda$  is an eigenvalue of the matrix of coefficients of the linearized system (e.g., Gelaro, 1987). Each eigenvalue  $\lambda$  represents one solution of the system. The sign of the real part of the eigenvalue determines the existence of the growth or the decay of its particular solution, and the magnitude of the real part determines the rate of this growth or decay. An eigenvalue with negative real part indicates exponential decay, a positive real part results in exponential growth, and a zero real part indicates neutral stability, neither growth nor decay. It is sufficient for any one real part of the set of eigenvalues to be positive for the system itself to be unstable (e.g., Gelaro, 1987). In the linear approximation, physical stability corresponds mathematically to the entire set of eigenvalues having negative real parts. Physical instability is initiated mathematically when any one of the real parts of the eigenvalues becomes positive. Zero real values of the eigenvalue therefore may reveal the changes of sign that in turn indicate changes in stability.

For values of time  $t$  near zero, solutions are said to be "near" the closest time-invariant stationary solution. For the linear solutions, the perturbations  $ce^{\lambda t}$  themselves are close to zero, and the solution approaches the stationary basic state. In this same neighborhood, the nonlinearities in

a nonlinear solution are products of very small quantities, effectively making them insignificant. In the vicinity of a stationary solution, the true nonlinear solution and the linear approximation are therefore asymptotic (e.g., Wiggins, 1990). The result is that the linear behavior of a solution is the same as the nonlinear behavior near a stationary solution. If a linear solution is stable or unstable near the stationary solution, then the nonlinear solution is correspondingly stable or unstable (e.g., Wiggins, 1990).

The real parts of the eigenvalues of the linear system consequently indicate the nonlinear local stability of the system. The presence of a single positive eigenvalue indicates linear and nonlinear instability. However, a problem arises for zero eigenvalues. A zero eigenvalue, which indicates neutral stability of the linear system, is indeterminate for the stability of the nonlinear system (e.g., Wiggins, 1990). Slight differences between the linear and nonlinear solutions near a stationary solution could "push" the stability of this particular solution either way. Only if the real parts of all eigenvalues of the linearized system are nonzero is the behavior of the linear approximation near a stationary solution the same as the nonlinear system (e.g., Wiggins, 1990).

In the physical system of the liquid melt, as well as in the nonlinear system modeling the flow and in its linear

approximation, the Rayleigh number is the critical parameter determining the flow regime stability (e.g., Krishnamurti, 1973). The Rayleigh number appears as a parameter in the eigenvalue equation, and it determines the sign of some of the eigenvalues. Critical Rayleigh numbers indicate the loss of stability of a stable solution, and they occur in sets of eigenvalues whose real parts are all negative, as the sign of any one real part changes to positive (e.g., Wiggins, 1990). This change in sign indicates a change in the stability of the system and a transition in the flow regimes. Although the real part of the eigenvalue is zero at this point and the linear approximation is not valid there, the critical Rayleigh number is the limit of stable and unstable solutions on either side that are valid. As the limit of such behaviors, it does indicate a change in stability.

In the linear perturbation of the system of ordinary differential equations for the conducting side wall, the basic state is convective flow, and the perturbation represents a small disturbance of this flow. In general, the basic state is a stationary flow or solution, and the perturbation is a function of time (e.g., Gelaro, 1987):

$$\psi_{54}(t) = \psi_{54}^S + \psi_{54}^P(t) \quad (5.24)$$

$$T_{34}(t) = T_{34}^S + T_{34}^P(t) \quad (5.25)$$

$$T_{03}(t) = T_{03}^S + T_{03}^P(t) \quad (5.26)$$

These are substituted into the nonlinear system,

$$\psi'_{54}(t) = -\frac{17868}{355} \text{Pr} \psi_{54}(t) + \frac{42}{71} \text{PrRa} T_{34}(t) \quad (5.27)$$

$$T'_{34}(t) = \psi_{54}(t) - \frac{138728}{4095} T_{34}(t) - \frac{28}{5} \psi_{54}(t) T_{03}(t) \quad (5.28)$$

$$T'_{03}(t) = -T_{03}(t) + \frac{777}{2048} \psi_{54}(t) T_{03}(t) \quad (5.29)$$

Only terms that are of the order of the perturbations are retained:

$$\psi^{P'}_{54}(t) = -\frac{17868}{355} \text{Pr} \psi^P_{54}(t) + \frac{42}{71} \text{PrRa} T^P_{34}(t) \quad (5.30)$$

$$T^{P'}_{34}(t) = \psi^P_{54}(t) - \frac{28}{5} T^S_{03} \psi^P_{54}(t) - \frac{138728}{4095} T^P_{34}(t) - \frac{28}{5} \psi^S_{54} T^P_{03}(t) \quad (5.31)$$

$$T^{P'}_{03}(t) = \frac{777}{2048} T^S_{34} \psi^P_{54}(t) + \frac{777}{2048} \psi^S_{54} T^P_{34}(t) - 48 T^P_{03}(t) \quad (5.32)$$

Note that the system is now expressed in the perturbation variables. The stability of these variables determines the stability of the entire system. It is the eigenvalues  $\lambda_i$  of this system that are to be investigated. It is more illustrative of the method to determine these by transforming the system into a system of variational equations than to find the eigenvalues directly (e.g., Gelaro, 1987). The system

above has perturbation solutions of the form:

$$\psi_{54}^P(t) = \hat{\psi}_{54} e^{\lambda t} \quad (5.34)$$

$$T_{34}^P(t) = \hat{T}_{34} e^{\lambda t} \quad (5.34)$$

$$T_{03}^P(t) = \hat{T}_{03} e^{\lambda t} \quad (5.35)$$

The effect of the sign of the eigenvalue on the growth of the perturbation is evident here. If these expressions are substituted into the linearized system, the variational equations become:

$$-\left(\frac{17868}{355} \text{Pr} + \lambda\right) \hat{\psi}_{54} + \frac{42}{71} \text{PrRa} \hat{T}_{34} = 0 \quad (5.36)$$

$$\left(1 - \frac{28}{5} T_{03}^S\right) \hat{\psi}_{54} - \left(\frac{138728}{4095} + \lambda\right) \hat{T}_{34} - \frac{28}{5} \hat{\psi}_{54} \hat{T}_{03}^S = 0 \quad (5.37)$$

$$\frac{777}{2048} T_{34}^S \hat{\psi}_{54} + \frac{777}{2048} \hat{\psi}_{54} \hat{T}_{34} - (48 + \lambda) \hat{T}_{03} = 0 \quad (5.38)$$

The system above allows determination of the eigenvalues for any stationary solution. In the present study the conductive stationary solution is of interest, and the system can be simplified considerably by letting the stationary solutions be the zero-convection solution:

$$-\left(\frac{17868}{355}\text{Pr} + \lambda\right)\psi_{54} + \frac{42}{71}\text{PrRa}\hat{T}_{34} = 0 \quad (5.39)$$

$$\psi_{54} - \left(\frac{138728}{4095} + \lambda\right)\hat{T}_{34} = 0 \quad (5.40)$$

$$(48 + \lambda)\hat{T}_{03} = 0 \quad (5.41)$$

For this system to have a nontrivial solution, the determinant of coefficients must be zero. The eigenvalue equation is a third degree polynomial in  $\lambda$ :

$$(48 + \lambda)\left[\lambda^2 + \lambda\left(\frac{17868\text{Pr}}{355} + \frac{138728}{4095}\right) + \frac{17868\text{Pr}}{355}\frac{138728}{4095} - \frac{42}{71}\text{PrRa}\right] = 0 \quad (5.42)$$

The eigenvalue solutions of this equation are:

$$\lambda_1 = -48 \quad (5.43)$$

$$\lambda_{2,3} = -\frac{1}{2}\left(\frac{17868\text{Pr}}{355} + \frac{138728}{4095}\right) \pm \frac{1}{2}\left[\left(\frac{17868\text{Pr}}{355} + \frac{138728}{4095}\right)^2 - 4\text{Pr}\left(\frac{17868}{355}\frac{138728}{4095} - \frac{42}{71}\text{Ra}\right)\right]^{\frac{1}{2}} \quad (5.44)$$

Eigenvalue  $\lambda_1$  is a constant, negative real number, indicating stability for its particular solution. Because the Prandtl number is always positive, the real part  $\lambda_3$  will always be negative, the radical being either a positive real number or a pure imaginary.

The sign of the real part of  $\lambda_2$ , however, depends upon the radicand. Because  $\lambda_2$  is of the form

$$-f_1 + \sqrt{f_1^2 - f_2} \quad (5.45)$$

the sign of the quantity

$$4\text{Pr}\left(\frac{17868}{355} \frac{138728}{4095} - \frac{42}{71}\text{Ra}\right) \quad (5.46)$$

determines the sign of the real part of  $\lambda_2$  and consequently the stability of the system. If this quantity is positive, which occurs for a Rayleigh number less than  $\sim 2882.5$ , the radical term will be either a positive real number less than

$$-\frac{1}{2}\left(\frac{17868\text{Pr}}{355} + \frac{138728}{4095}\right) \quad (5.47)$$

or an imaginary number, and the real part of  $\lambda_2$  will be negative. In this case, all the eigenvalues are negative and the system is stable. If the quantity is negative, for a Rayleigh number greater than  $\sim 2882.5$ , then the radicand will be a positive number such that the real part of  $\lambda_2$  will be positive. The system is then unstable. This value of  $\sim 2882.5$  is the first critical Rayleigh number for the conducting side wall case. The condition that the critical Rayleigh number be at the change in sign of the real part of the eigenvalue has been met. The supposition in section 5.2 concerning the value of the critical Rayleigh number based on the stationary solutions was correct.

It is evident that the Prandtl number has no effect on the sign of  $\lambda_2$  or changes in the stability of the system. Therefore the change in stability is a function of the shape of the container and not of the fluid properties. In this linear model of stability, the Prandtl number does however have an effect on the rate of growth of the convective perturbation near the instability. The higher the Prandtl number, the larger the positive real eigenvalue and the greater the growth of the perturbation.

The behavior of the system with respect to the transition between stationary solutions may be seen easily in the bifurcation diagrams of the stationary solutions for the stream function and temperature temporal coefficients (Figs. 22, 23, and 24).

The procedure for determining the critical Rayleigh number is repeated for the case of insulated sides (see Appendix A for the calculations). After considerable algebra, the critical Rayleigh number in this case is found to be  $\sim 2331.6$ . The bifurcation diagrams are much the same as those for the conducting side wall case (Figs. 25, 26, and 27). This lower value of the critical Rayleigh number validates the model's treatment of the thermal boundary conditions. From a physical perspective, the lower value for the instability here indicates that less of a temperature gradient is required to destabilize the fluid column. This is exactly the case for

the insulated side wall, through which there is no heat loss.

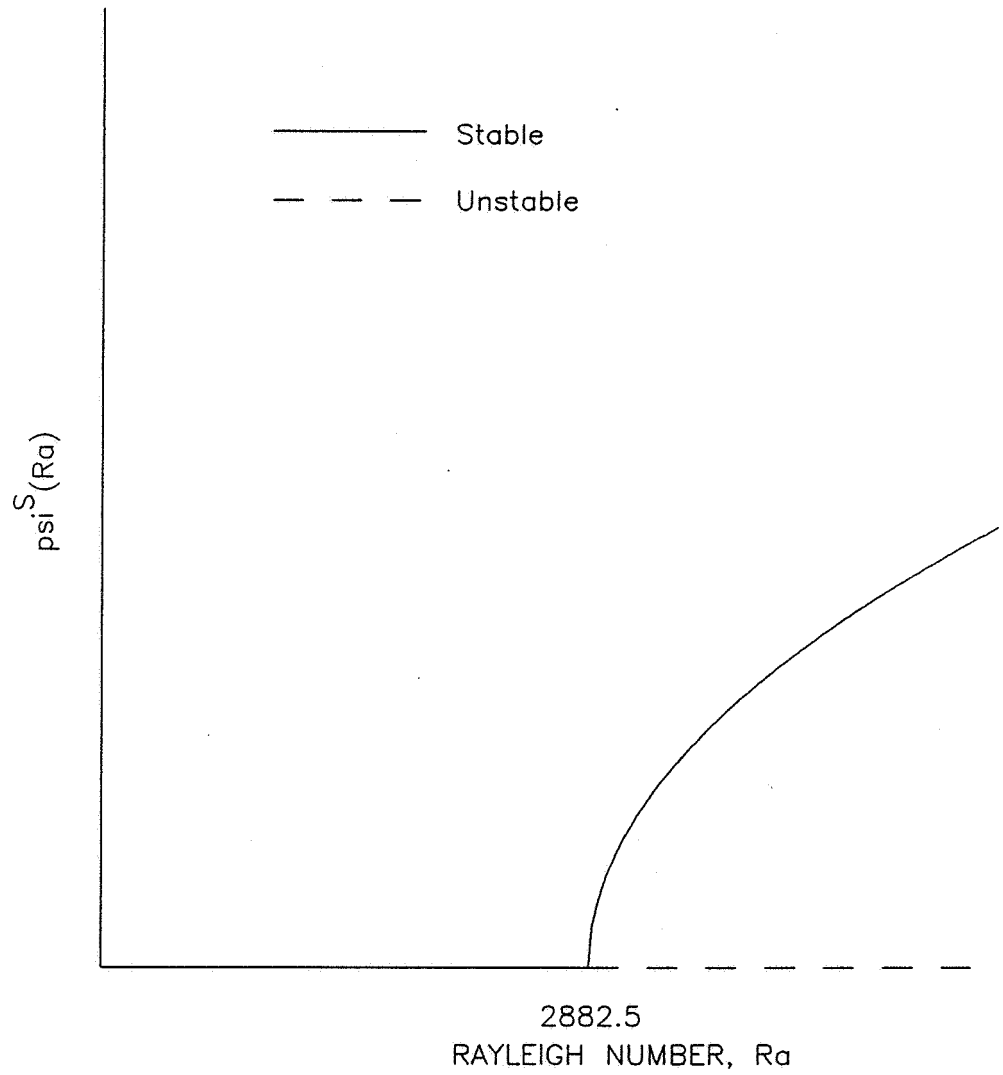


**Figure 22.** Bifurcation diagram for  $\psi_{54}(t)$ , conducting side wall.

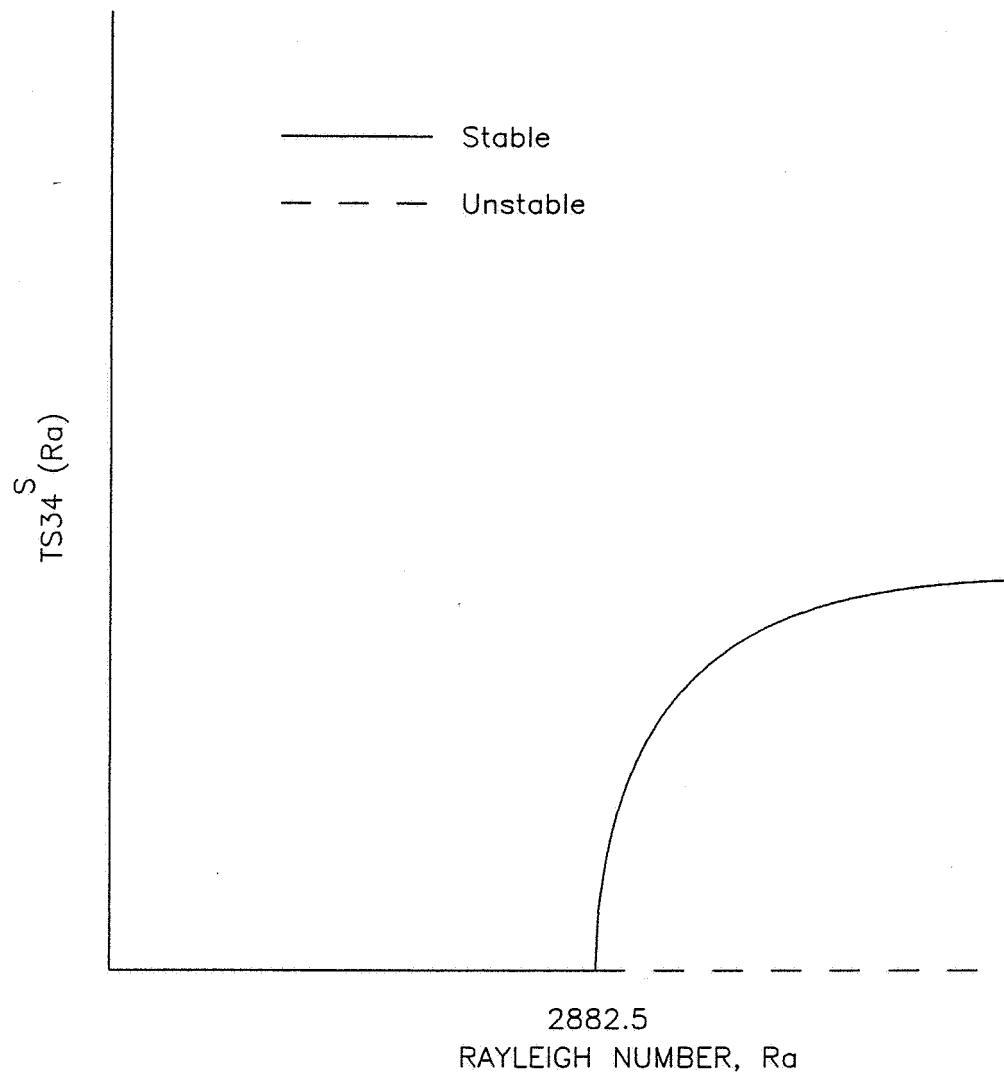


**Figure 23.** Bifurcation diagram for  $T_{34}(t)$ , conducting side wall.

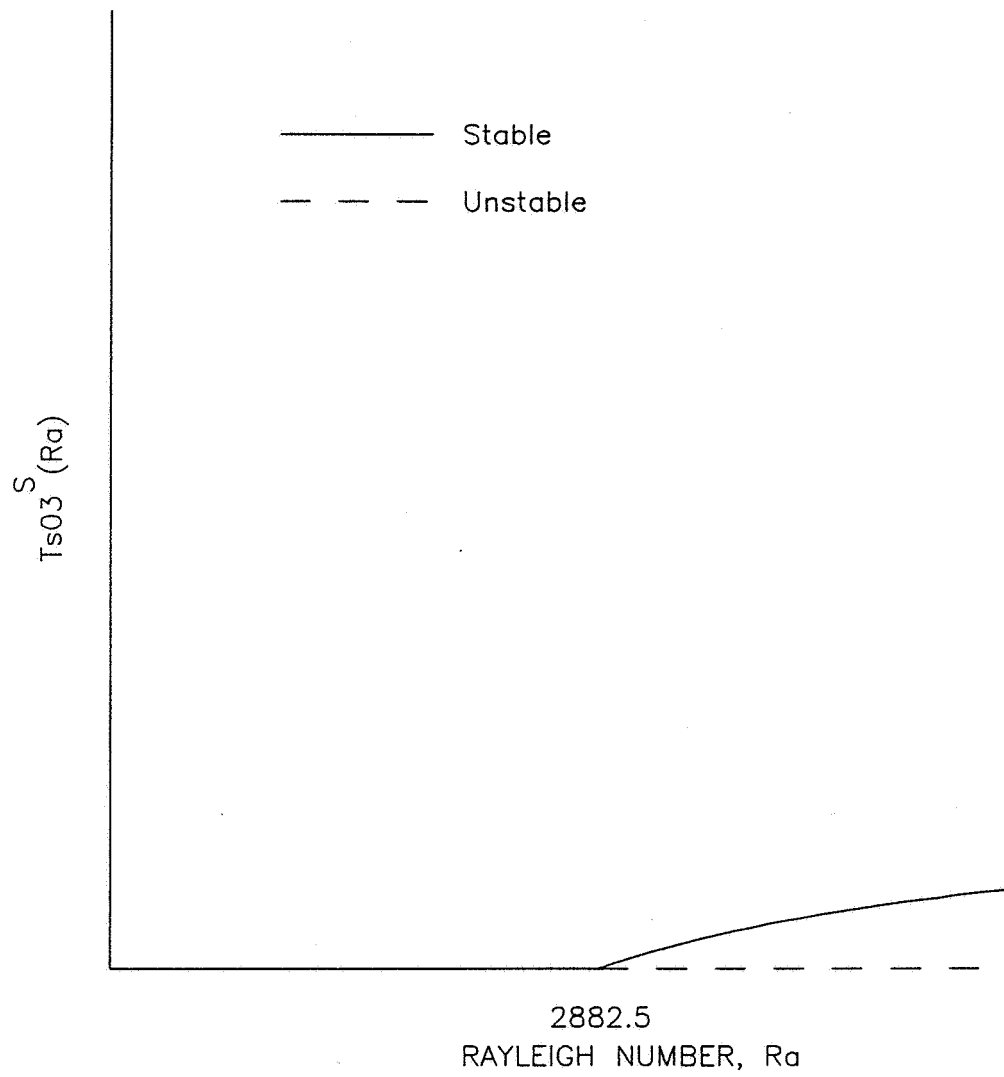


**Figure 24.** Bifurcation diagram for  $T_{03}(t)$ , conducting side wall.

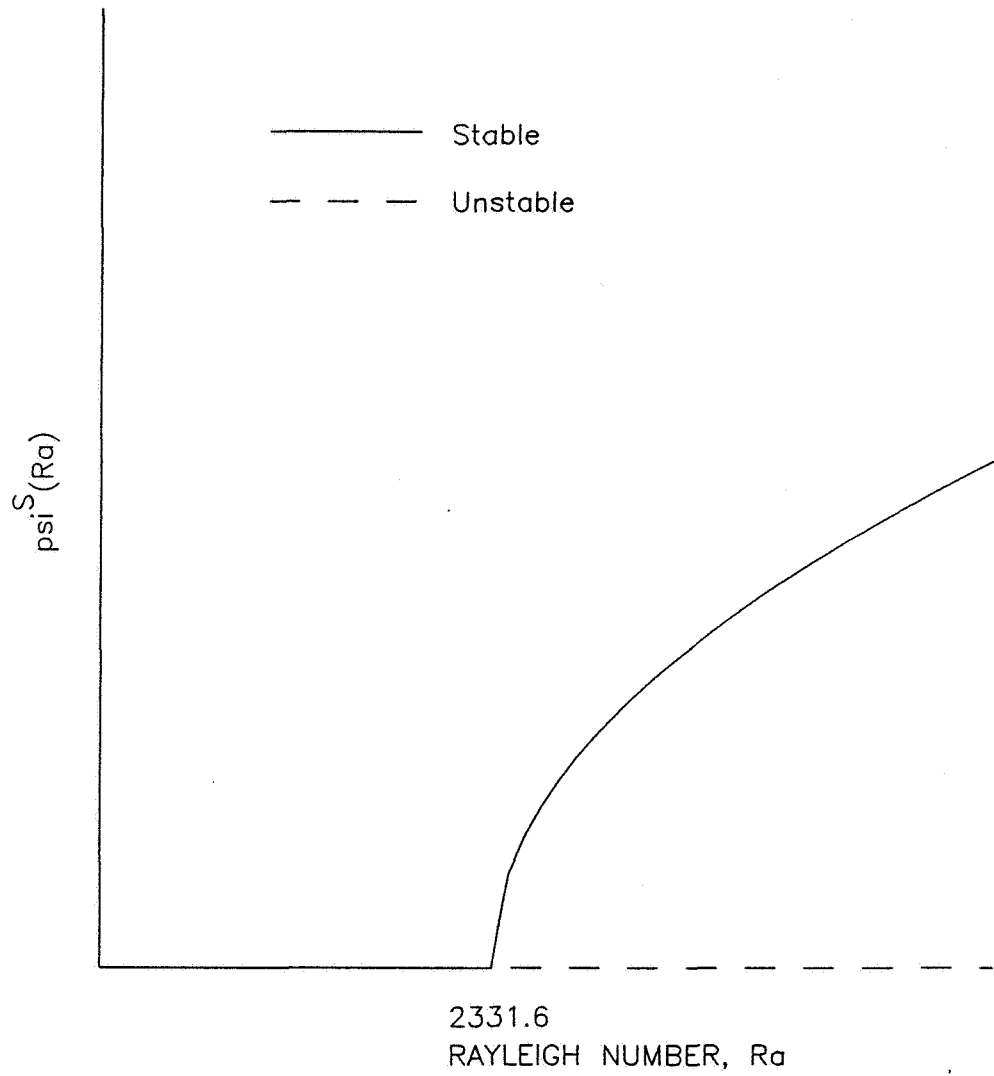


**Figure 25.** Bifurcation diagram for  $\psi_{54}(t)$ , insulated side wall.

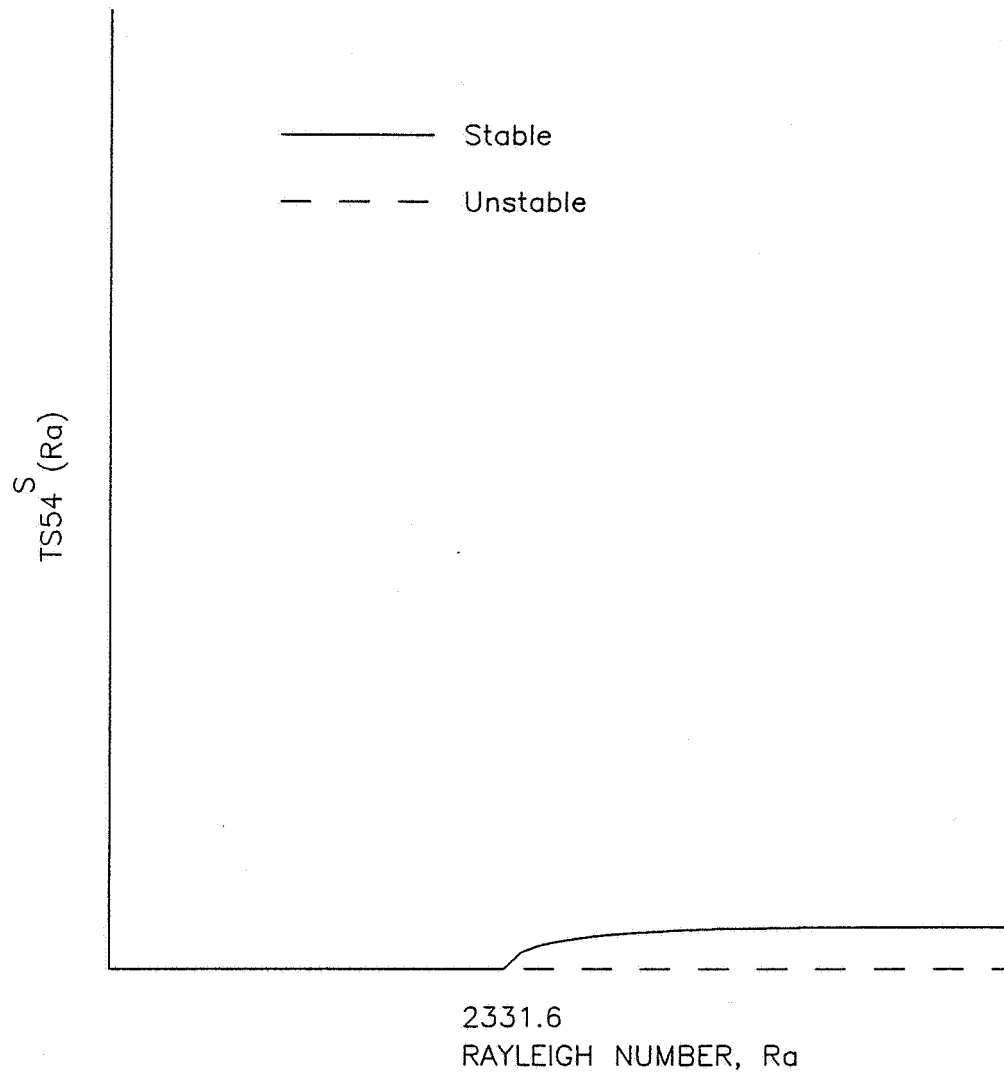


**Figure 26.** Bifurcation diagram for  $T_{54}(t)$ , insulated side wall.

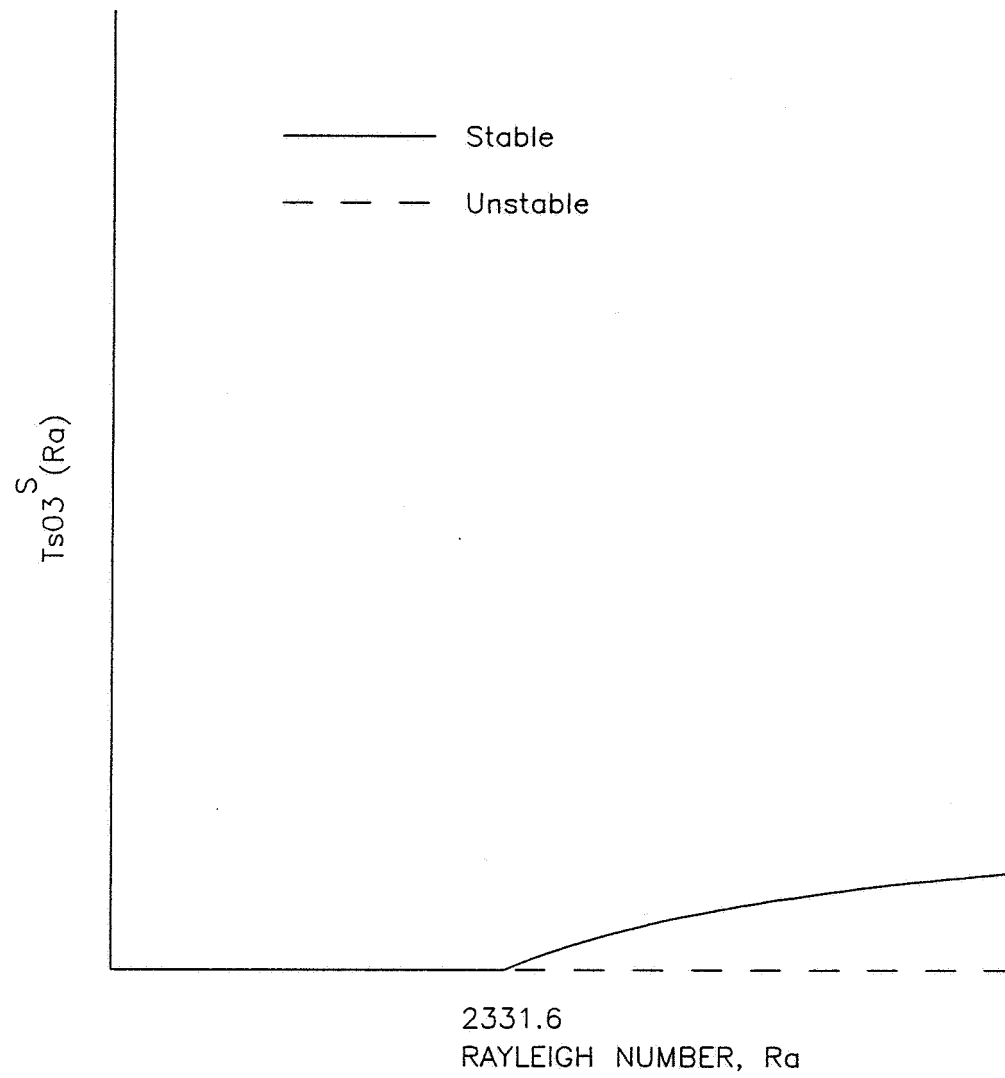


**Figure 27.** Bifurcation diagram for  $T_{03}(t)$ , insulated side wall.

## CHAPTER 6. DISCUSSION OF RESULTS

The Chebyshev-Galerkin spectral model of Rayleigh-Bénard convection in this study is formulated upon, and exhibits, certain features that have been observed in experiments. Axisymmetric flow is found in cylinders of equal height and radius (e.g., Müller et al., 1984). The convergence of this type of flow at the center of the cylinder moves the center of rotation of the single convection cell outward past  $R/2$ , the midpoint of the radius (e.g., Müller et al., 1984). Although the behavior of a low-Prandtl number fluid is investigated in this study, both experiment and the model itself demonstrate the Prandtl number independence of the first critical Rayleigh number (Krishnamurti, 1973).

The results for the first critical Rayleigh number from this study are both slightly higher than those found by Charlson and Sani (1970) in their Rayleigh-Ritz formulation for the same problem. For the conducting side wall, the value of 2882.5 is 13.3% higher than their value of 2545.0, and for the insulated side wall, the value of 2331.6 is 3.1% higher than their value of 2261.9.

The experimental value of the first critical Rayleigh number for liquid gallium determined by Müller et al. (1984) had to be interpolated from their graph (Fig. 28) for their aspect ratio of  $h/d=0.5$  ( $\gamma=1$ ) because the authors did not

state the exact numerical result. Interpolation from the graph gives a value for  $Ra_{C1}$  of approximately 2700 for the Bridgman configuration (insulated side wall). Although the value of 2331.6 from the present study differs by 13.6% from this experiment, it is closer than that found by Charlson and Sani (1970).

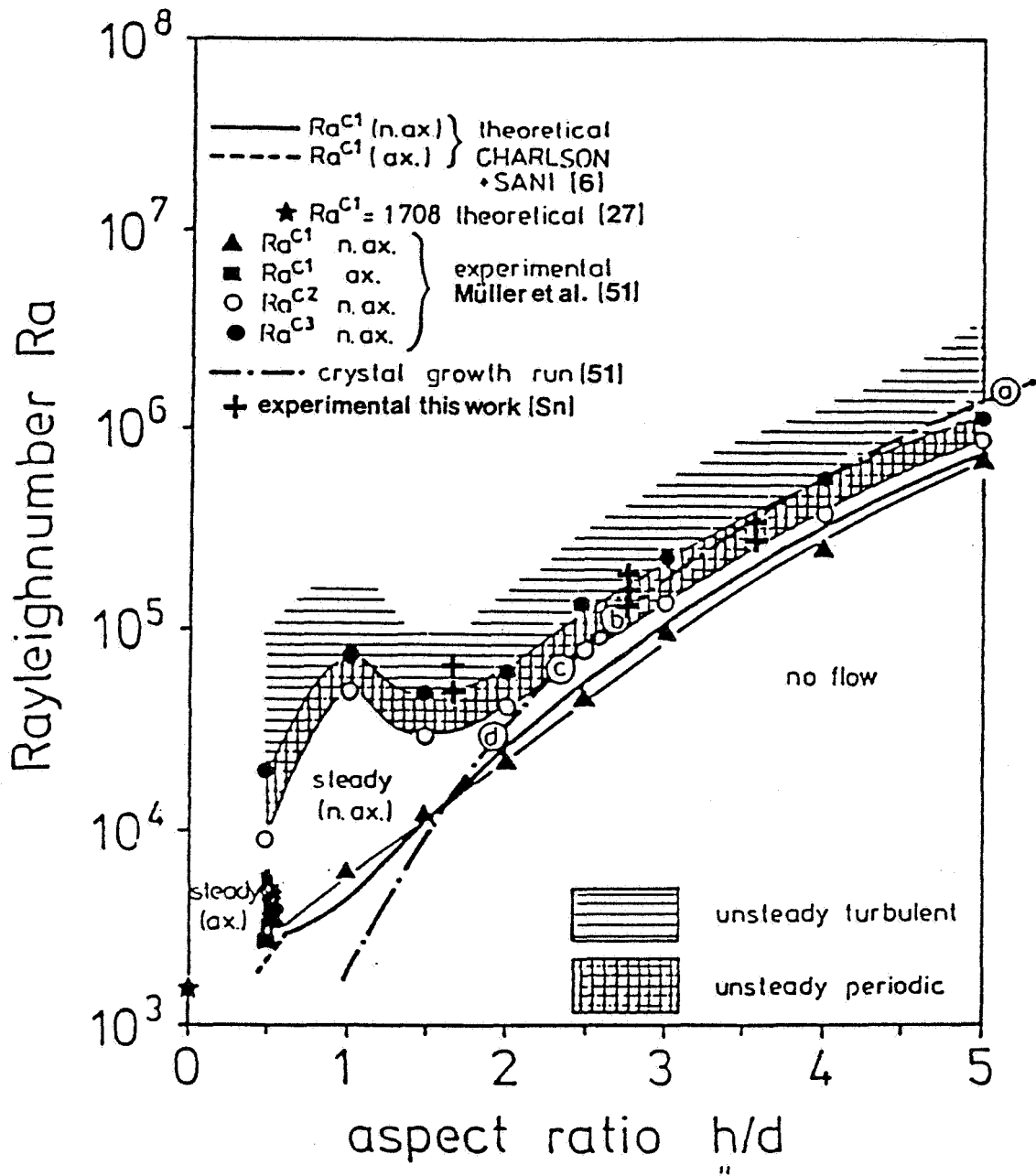


**Figure 28.** Graph from Müller et al. (1984) showing the flow regimes and transitions for liquid gallium.

## CHAPTER 7. CONCLUSION

In this study, the onset of laminar axisymmetric Rayleigh-Bénard convection is investigated for a fluid in a cylindrical container whose radius is equal to its height. A simplified model of the vertical Bridgman crystal growth configuration is used. Two different cases are considered for the thermal boundary conditions at the side wall: conducting and insulated surfaces. All surfaces are assumed to be solid and no-slip.

The governing Boussinesq system is first perturbed. It is then simplified by introducing a Stokes stream function and by taking the curl of the Navier-Stokes equations. A Chebyshev-Galerkin spectral model reduces the simplified system to a system of first-order ordinary differential equations. A local stability analysis using the linearized system determines the two values of the first critical Rayleigh number for the insulated and conducting side walls.

Although this study investigates the onset of laminar convection for a low-Prandtl number liquid metal in a cylinder with equal radius and height, the results are more general. The critical Rayleigh number at this transition is independent of the Prandtl number, so that the  $Ra_{c1}$  values obtained here are valid for all fluids within the parameters of the formulation. Furthermore, the presence of a single convection

cell in cylinders of aspect ratio higher than the value of one in this study (e.g., Tritton, 1988) suggests that the model is applicable to the determination of  $Ra_{c1}$  for these high-aspect ratio cylinders.

The relative magnitudes of the first critical Rayleigh number values that are obtained, 2882.5 for the conducting side wall and 2331.6 for the insulated case, tend to validate the method. The  $Ra_{c1}$  for the conducting side wall should be higher than that for the insulated side wall, the heat lost through the conducting surface not being available to initiate the flow transition.

The approach used in this study results in a value of  $Ra_{c1}$  for the case of the insulated side wall that is closer than that of the numerical work of Charlson and Sani (1970) to the experimental value determined by Müller et al. (1984).

A more precise approach to the problem presented in this study would be to determine the flow and temperature distributions in the laminar convective regime by some numerical method rather than by curve-fitting. These distributions could be approximated by polynomials and Chebyshev series. The rest of the procedure would be the same.

The procedure used in Chapter 5 to determine the first critical Rayleigh number may also be used to determine the second critical Rayleigh number. In this case the nonzero

laminar convective stationary solutions are used in the linearized system and its eigenvalue equation. Although the eigenvalue equation is a numerically more complicated cubic, its solution is still possible (e.g., Gelaro, 1987).

The Chebyshev-Galerkin spectral method used in this study to determine the first critical Rayleigh number for a low-Prandtl number crystal melt must be modified to find the full sequence of critical Rayleigh numbers. The Chebyshev series expressions for the stream function and the temperature need to be considerably longer to account for the increased number of flow modes or length scales that need to be represented as the flow become more turbulent. These expressions must also allow inclusion of the inertial term of the Navier-Stokes equation to account for the strong nonlinearity for any non-zero velocity field. A serious problem with the extrapolation of the specific method used here is the difficulty of satisfying the boundary conditions. The coefficients of the spatial distributions in the present study could be chosen to satisfy the boundary conditions because there was only one simple flow field to model. If these coefficients are unknown, the boundary conditions are not automatically satisfied and impose added constraints.

## REFERENCES

- Argyris, J., Faust, G., and Haase, M. (1991). "Χαος, an adventure in chaos." *Computer Methods in Applied Mechanics and Engineering* 91, 997-1091.
- Bénard, H. (1900). "Les tourbillons cellulaires dans une nappe liquide." *Revue Générale des Sciences Pures et Appliquées* 11, 1261-1271.
- Bénard, H. (1901). "Les tourbillons cellulaires dans une nappe liquide transportant de la chaleur par convection en régime permanent." *Annales de Chimie et de Physique* 23, 62-144.
- Bergé, P., Pomeau, Y., and Vidal, C. (1984). *Order Within Chaos*. John Wiley & Sons, Inc., New York, N.Y.
- Block, M.J. (1956). "Surface tension as the cause of Bénard cells and surface deformation in a liquid film." *Nature* 178, 650-651.
- Boussinesq, J. (1903). *Théorie Analytique de la Chaleur*, Vol. 2. Gauthier-Villars, Paris.
- Canuto, C., Hussaini, M.Y., Quarteroni, A., and Zang, T.A. (1990). *Spectral Methods in Fluid Mechanics*. Springer-Verlag, New York, N.Y.
- Carlson, F.M., Fripp, A.L., and Crouch, R.K. (1984). "Thermal convection during Bridgman crystal growth." *Journal of Crystal Growth* 68, 747-756.
- Chandrasekhar, S. (1961). *Hydrodynamic and hydromagnetic stability*. Clarendon Press, Oxford.
- Charlson, G.S. and Sani, R.L. (1970). "Thermoconvective instability in a bounded cylindrical fluid layer." *International Journal of Heat and Mass Transfer* 13, 1479-1496.
- Crouch, R.K., Fripp, A.L., Debnam, W.J., Clark, I.O., Barber, P.G., and Carlson, F.M. (1985). "Experimental investigation of the effects of gravity on thermosolutal convection and compositional homogeneity in Bridgman grown, compound semiconductors." *Acta Astronautica* 12, 923-929.
- Davis, S.H. (1968). "Convection in a box: on the dependence of preferred wave-number upon the Rayleigh number at finite amplitude." *Journal of Fluid Mechanics* 32, 619-624.

- Deane, A.E. and Sirovich, L. (1991). "A computational study of Rayleigh-Bénard convection. Part 1. Rayleigh-number Scaling." *Journal of Fluid Mechanics* 222, 231-250.
- Drazin, P.G. and Reid, W.H. (1981). *Hydrodynamic Stability*. Cambridge University Press, Cambridge.
- Gelaro, R. (1987). "Linear stability analysis," in: *Nonlinear Hydrodynamic Modeling: A Mathematical Introduction*, Ed. H.N. Shiner, Springer-Verlag, New York, N.Y.
- Gleick, J. (1988). *Chaos: Making a New Science*. Penguin Books, New York, N.Y.
- Haldenwang, P. (1986). "Unsteady numerical simulation by Chebyshev spectral methods of natural convection at high Rayleigh number." Proceedings of the 1986 ASME Winter Annual Meeting, "Significant Questions in Buoyancy-Affected Enclosures or Cavity Flows," Anaheim, CA, 45-51.
- Higgins, R.W. (1987). "From the equations of motion to spectral models," in: *Nonlinear Hydrodynamic Modeling: A Mathematical Introduction*, Ed. H.N. Shiner, Springer-Verlag, New York, N.Y.
- Horsch, G.M. (1988). "Cooling-induced convective littoral currents in lakes," dissertation presented to the University of Minnesota, in partial fulfillment of the requirements for the Degree of Doctor of Philosophy.
- Kim, K.M., Witt, A.F., and Gatos, H.C. (1972). "Crystal growth from the melt under destabilizing thermal gradients." *J. Electrochem. Soc.* 119, 1218.
- Knuteson, D.J. (1989). "Experimental study of convection in tin in a vertical Bridgman configuration," dissertation presented to the Department of Chemical Engineering, University of Florida, in partial fulfillment of the requirements for the Degree of Doctor of Philosophy.
- Koschmieder, E. (1966). "On convection on a uniformly heated rotating plane." *Beitr. Phys. Atmos.* 39, 1-11.
- Koschmieder, E. (1967). "On convection on a uniformly heated rotating plane." *Beitr. Phys. Atmos.* 40, 216-225.
- Koschmieder, E. (1969). "On the wavelength of convective motions." *J. Fluid Mech.* 350, 527-530.

- Krishnamurti, R. (1970a). "On the transition to turbulent convection. Part 1." *Journal of Fluid Mechanics* 42, 295-307.
- Krishnamurti, R. (1970b). "On the transition to turbulent convection. Part 2." *Journal of Fluid Mechanics* 42, 309-320.
- Krishnamurti, R. (1973). "Some further studies on the transition to turbulent convection." *Journal of Fluid Mechanics* 60, 285-303.
- Le Queré, P. and Alziary de Roquefort, T. (1985). "Computation of natural Convection in two-dimensional cavities with Chebyshev polynomials." *Journal of Computational Physics* 57, 210-228.
- Liang, S.F., Vidal, A., and Acrivos, A. (1969). "Buoyancy-driven convection in cylindrical geometries." *Journal of Fluid Mechanics* 32, 619-624.
- Lorenz, E.N. (1963). "Deterministic nonperiodic flow." *J. Atmos. Sci.* 20, 130-141.
- Müller, G., Neumann, G., and Weber, W. (1984). "Natural convection in vertical Bridgman configurations", *Journal of Crystal Growth* 70, 78-93.
- Mullins, W.W. and Sekarka, R.F. (1964). "Stability of a planar interface during solidification of a dilute binary alloy." *J. Appl. Phys.* 35, 444.
- Nese, J.N. (1987). "The transition to turbulence," in: *Nonlinear Hydrodynamic Modeling: A Mathematical Introduction*, Ed. H.N. Shrier, Springer-Verlag, New York, N.Y.
- Orszag, S.A. (1971a). "Numerical simulation of incompressible flows within simple boundaries. I. Galerkin (spectral) representations." *Studies in Applied Mathematics* L(4), 293-327.
- Orszag, S.A. (1971b). "Galerkin approximations to flows within slabs, spheres, and cylinders." *Physical Review Letters* 26(18), 1100-1103.
- Ostrach, S. (1985). "Fluid mechanics in crystal growth--The 1982 Freeman Scholar Lecture", *Journal of Fluids Engineering* 105, 5-20.
- Ostrach, S., and Pnueli, D. (1963). "The thermal instability of completely confined fluids inside some particular

configurations" *Journal of Heat Transfer* 85, 1346-1354.

Parker, S.G. and Johnson, R.E. (1981) in: *Preparation and Properties of Solid State Materials*, Eds. W.R. Wilcox and R.A. Levever, Marcel Dekker, New York, N.Y.

Pearson, J.R.A. (1958). On convective cells induced by surface tension." *Journal of Fluid Mechanics* 4, 489-500.

Pellew, A. and Southwell, R.V. (1940). "On maintained convective motion in a fluid heated from below." *Proc. R. Soc.* 176A, 312-343.

Lord Rayleigh (1916). "On convective currents in a horizontal layer of fluid when the higher temperature is on the under side." *Phil. Mag.* 32, 529-546.

Saltzman, B. (1962). "Finite amplitude free convection as an initial value problem--I." *J. Atmos. Sci.* 19, 329-341.

Segel, L.A. (1969). "Distant side-walls cause slow-amplitude modulation of cellular convection." *Journal of Fluid Mechanics* 38, 293-324.

Shirer, H.N. (1987). "A simple nonlinear model of convection," in: *Nonlinear Hydrodynamic Modeling: A Mathematical Introduction*, Ed. H.N. Shirer, Springer-Verlag, New York, N.Y.

Tarman, I.H. (1989). "Analysis of turbulent thermal convection," dissertation presented to the Department of Applied Mathematics, Brown University, in partial fulfillment of the requirements for the Degree of Doctor of Philosophy.

Thompson, J.M.T. and Stewart, H.B. (1986). *Nonlinear Dynamics and Chaos*. John Wiley & Sons Ltd., Chichester.

Tiller, W.A., Jackson, K.A., Rutter, J.W., and Chalmers, B. (1953). "The redistribution of solute atoms during the solidification of metals." *Acta Metallurgica* 1, 428.

Tritton, D.J. (1988). *Physical Fluid Dynamics*, 2nd ed. Clarendon Press, Oxford.

Wiggins, S. (1990). *Introduction to Applied Nonlinear Systems and Chaos*. Springer-Verlag, New York, N.Y.

Zierep, J. (1963). "Zur Theorie der Zellularkonvektion V." *Beitr. Phys. Atmos.* 36, 70-76.

## APPENDIX A. LOCAL STABILITY ANALYSIS, INSULATED SIDE WALL

The local stability analysis of the system of nonlinear ordinary differential equations obtained in Chapter 4 for the case of the insulated side wall is similar to that for the conducting side wall. The system is perturbed about the conductive stationary solution and is linearized. The first critical Rayleigh number is determined from the eigenvalue equation of the linearized system. The procedure follows that of Gelaro (1987).

In the determination of the local stability of a stationary convective solution, the basic state is the stationary convective flow, and the temporal perturbation represents a small disturbance of this flow. As in the case of the conducting side wall, the independent variables for the insulated side wall are represented by first-order expansions:

$$\psi_{54}(t) = \psi_{54}^S + \psi_{54}^P(t) \quad (\text{A.1})$$

$$T_{54}(t) = T_{54}^S + T_{54}^P(t) \quad (\text{A.2})$$

$$T_{03}(t) = T_{03}^S + T_{03}^P(t) \quad (\text{A.3})$$

These expressions are substituted into the nonlinear system derived for the case of the insulated side wall (eqns. 4.92-4.94),

$$\psi'_{54}(t) = -\frac{17868}{355} \text{Pr} \psi_{54}(t) + \frac{2765}{426} \text{PrRa} T_{54}(t) \quad (\text{A.4})$$

$$T'_{54}(t) = \frac{114636}{1205993} \psi_{54}(t) - \frac{38915152}{1361605} T_{54}(t) - \frac{3209800}{6029965} \psi_{54}(t) T_{03}(t) \quad (\text{A.5})$$

$$T'_{03}(t) = -48 T_{03}(t) + \frac{63805}{16384} \psi_{54}(t) T_{54}(t) \quad (\text{A.6})$$

The resulting system is linearized by retaining only those terms of the order of the perturbations:

$$\psi^{P'}_{54}(t) = -\frac{17868}{355} \text{Pr} \psi^P_{54}(t) + \frac{2765}{426} \text{PrRa} T^P_{54}(t) \quad (\text{A.7})$$

$$T^{P'}_{54}(t) = \frac{114636}{1205993} \psi^P_{54}(t) - \frac{3209800}{6029965} T^S_{03} \psi^P_{54}(t) - \frac{38915152}{6029965} T^P_{54}(t) - \frac{3209800}{6029965} \psi^S_{54} T^P_{03}(t) \quad (\text{A.8})$$

$$T^{P'}_{03}(t) = \frac{63805}{16384} T^S_{54} \psi^P_{54}(t) + \frac{63805}{16384} \psi^S_{54} T^P_{54}(t) - 48 T^P_{03}(t) \quad (\text{A.9})$$

This system of first-order ordinary differential equations has exponential solutions of the form:

$$\psi^P_{54}(t) = \psi_{54} e^{\lambda t} \quad (\text{A.10})$$

$$T^P_{54}(t) = \hat{T}_{54} e^{\lambda t} \quad (\text{A.11})$$

$$T^P_{03}(t) = \hat{T}_{03} e^{\lambda t} \quad (\text{A.12})$$

Substitution of these expressions into the linearized system yields the variational system of equations:

$$-\left(\frac{17868}{355}\text{Pr} + \lambda\right)\psi_{54} + \frac{2765}{426}\text{PrRa}\hat{T}_{34} = 0 \quad (\text{A.13})$$

$$\left(\frac{114636}{1205993} - \frac{3209800}{6029965}T_{03}^S\right)\psi_{54} - \left(\frac{38915152}{1361605} + \lambda\right)\hat{T}_{54} - \frac{3209800}{6029965}\psi_{54}^S\hat{T}_{03} = 0 \quad (\text{A.14})$$

$$\frac{63805}{16384}T_{34}^S\psi_{54} + \frac{63805}{16384}\psi_{54}^S\hat{T}_{34} - (48 + \lambda)\hat{T}_{03} = 0 \quad (\text{A.15})$$

The system above allows determination of the eigenvalues for any stationary solution. In the present study, the stability of the conductive stationary solution for the insulated side wall,

$$\psi_{54}^S = 0, T_{54}^S = 0, T_{03}^S = 0 \quad (\text{A.16})$$

is of interest, and the system can be simplified by letting the stationary solutions be this zero-convection solution:

$$-\left(\frac{17868}{355}\text{Pr} + \lambda\right)\psi_{54} + \frac{2765}{426}\text{PrRa}\hat{T}_{54} = 0 \quad (\text{A.17})$$

$$\frac{114636}{1205993}\psi_{54} - \left(\frac{38915152}{1361605} + \lambda\right)\hat{T}_{54} = 0 \quad (\text{A.18})$$

$$(48 + \lambda)\hat{T}_{03} = 0 \quad (\text{A.19})$$

For this system to have a nontrivial solution, the determinant of coefficients must be zero. This eigenvalue equation is a

third degree polynomial in  $\lambda$ :

$$(48 + \lambda) \left[ \lambda^2 + \lambda \left( \frac{17868\text{Pr}}{355} + \frac{38915152}{1361605} \right) + \frac{17868\text{Pr}}{355} \frac{38915152}{1361605} - \left( \frac{2765}{426} \right) \left( \frac{114636}{1205993} \right) \text{PrRa} \right] = 0 \quad (\text{A.20})$$

The signs of the real parts of the eigenvalue solutions of this equation determine the stability of the system. If the real parts of all the eigenvalues are negative, then all linear perturbations decay, and the system is stable. If the real part of any one eigenvalue is positive, its particular perturbation solution grows without bound, making the whole system unstable. The transition from stability to instability occurs at the change in sign of a single real part in a set of negative real parts. The first critical Rayleigh number, which marks this transition from stability to instability, is found by varying the Ra parameter to obtain the first zero real part at which the sign changes.

The eigenvalue solutions of the above equation are:

$$\lambda_1 = -48 \quad (\text{A.21})$$

$$\lambda_{2,3} = -\frac{1}{2} \left( \frac{17868\text{Pr}}{355} + \frac{38915152}{1361605} \right) \pm \frac{1}{2} \left[ \left( \frac{17868\text{Pr}}{355} + \frac{38915152}{1361605} \right)^2 - 4\text{Pr} \left( \frac{17868}{355} \frac{38915152}{1361605} - \frac{2765}{426} \frac{114636}{1205993} \text{Ra} \right) \right]^{\frac{1}{2}} \quad (\text{A.22})$$

Eigenvalue  $\lambda_1$  is a constant negative real number, indicating

stability for its particular solution. Because the Prandtl number is always positive, the real part of  $\lambda_3$  will always be negative, the radical being either a positive real number or a pure imaginary.

The sign of the real part of  $\lambda_2$ , however, depends upon the radicand. Because  $\lambda_2$  is of the form

$$-f_1 + \sqrt{f_1^2 - f_2} \quad (\text{A.23})$$

the sign of the quantity

$$4\text{Pr} \left[ \left( \frac{17868}{355} \right) \left( \frac{38915152}{1361605} \right) - \left( \frac{2765}{426} \right) \left( \frac{114636}{1205993} \right) \text{Ra} \right] \quad (\text{A.24})$$

determines the sign of the real part of  $\lambda_2$  and consequently the stability of the system. If this quantity is positive, which occurs for a Rayleigh number less than ~2331.6, the radical term will be either a positive real number less than

$$-\frac{1}{2} \left( \frac{17868\text{Pr}}{355} + \frac{38915152}{1361605} \right) \quad (\text{A.25})$$

or an imaginary number, and the real part of  $\lambda_2$  will be negative. In this case, all the eigenvalues are negative and the system is stable. If the quantity is negative, for a Rayleigh number greater than ~2331.6, then the radicand will be a positive number such that the real part of  $\lambda_2$  will be positive. The system is then unstable. This value of ~2331.6 is the first critical Rayleigh number for the insulated side wall case. The condition that the critical Rayleigh number be

at the change in sign of the real part of the eigenvalue has been met. The supposition in section 5.2 concerning the value of the critical Rayleigh number based on the stationary solutions (eqs. 5.17-5.19 and 5.20-5.22) has again been shown to be correct. In this case also, the first critical Rayleigh number is independent of the Prandtl number.